New Mexico Geological Society

Downloaded from: https://nmgs.nmt.edu/publications/guidebooks/67



Stratigraphy, gravel provenance, and age of early Rio Grande deposits exposed 1-2 km northwest of downtown Truth or Consequences, New Mexico

Daniel J. Koning, Andrew P. Jochems, Gary S. Morgan, Virgil Lueth, and Lisa Peters
2016, pp. 459-478. https://doi.org/10.56577/FFC-67.459
Supplemental data: https://nmgs.nmt.edu/repository/index.cfml?rid=2016005

in:

Guidebook 67 - Geology of the Belen Area, Frey, Bonnie A.; Karlstrom, Karl E. ; Lucas, Spencer G.; Williams, Shannon; Zeigler, Kate; McLemore, Virginia; Ulmer-Scholle, Dana S., New Mexico Geological Society 67th Annual Fall Field Conference Guidebook, 512 p. https://doi.org/10.56577/FFC-67

This is one of many related papers that were included in the 2016 NMGS Fall Field Conference Guidebook.

Annual NMGS Fall Field Conference Guidebooks

Every fall since 1950, the New Mexico Geological Society (NMGS) has held an annual Fall Field Conference that explores some region of New Mexico (or surrounding states). Always well attended, these conferences provide a guidebook to participants. Besides detailed road logs, the guidebooks contain many well written, edited, and peer-reviewed geoscience papers. These books have set the national standard for geologic guidebooks and are an essential geologic reference for anyone working in or around New Mexico.

Free Downloads

NMGS has decided to make peer-reviewed papers from our Fall Field Conference guidebooks available for free download. This is in keeping with our mission of promoting interest, research, and cooperation regarding geology in New Mexico. However, guidebook sales represent a significant proportion of our operating budget. Therefore, only *research papers* are available for download. *Road logs*, *mini-papers*, and other selected content are available only in print for recent guidebooks.

Copyright Information

Publications of the New Mexico Geological Society, printed and electronic, are protected by the copyright laws of the United States. No material from the NMGS website, or printed and electronic publications, may be reprinted or redistributed without NMGS permission. Contact us for permission to reprint portions of any of our publications.

One printed copy of any materials from the NMGS website or our print and electronic publications may be made for individual use without our permission. Teachers and students may make unlimited copies for educational use. Any other use of these materials requires explicit permission.

This page is intentionally left blank to maintain order of facing pages.

New Mexico Geological Society Guidebook, 67th Field Conference, Geology of the Belen Area, 2016, p. 459-478.

STRATIGRAPHY, GRAVEL PROVENANCE, AND AGE OF EARLY RIO GRANDE DEPOSITS EXPOSED 1-2 KM NORTHWEST OF DOWNTOWN TRUTH OR CONSEQUENCES, NEW MEXICO

Daniel J. Koning[1], Andrew P. Jochems[1], Gary S. Morgan[2], Virgil Lueth[1], and Lisa Peters[1]

[1]*New Mexico Bureau of Geology and Mineral Resources, 801 Leroy Place, Socorro, NM, 87801; dkoning@nmbg.nmt.edu*
[2]*New Mexico Museum of Natural History and Science, 1801 Mountain Rd. NW, Albuquerque, NM 87104*

Abstract—Within 2 km northwest of downtown Truth or Consequences, the discovery of a fossil tooth identified as *Neohipparion eurystyle* and $^{40}Ar/^{39}Ar$ dating of cryptomelane in a fault zone indicate that a through-going, ancestral Rio Grande became established in the Engle and northern Palomas basins prior to 4.87 Ma (best estimate of 5.0 to 5.5? Ma). In the lower ~25 m of the ancestral Rio Grande deposits, referred to as the lower coarse unit (LCU), we differentiate three gravel-based petrofacies units. Gravel of the basal 3-5 m of the LCU in the southeastern part of the study area (petrofacies unit 1) consists almost entirely of Paleozoic and Mesozoic sedimentary rocks inferred to be derived from toe-cutting of the nearby Mescal-Ash Canyon paleofan during establishment of the ancestral Rio Grande. Gravel in the overlying petrofacies unit 2 is composed of felsic volcanic rocks plus minor Proterozoic clasts and Mesozoic-Paleozoic sedimentary clasts, reflecting mixing of gravel shed from highlands surrounding the Engle basin. Only petrofacies unit 3 contains notable exotic clasts transported by the ancestral Rio Grande, namely 10-40% quartzite and trace Pedernal chert, that are mixed with roughly subequal felsic and intermediate volcanic types shed from highlands located west-northwest of the study area. Stratigraphic relationships coupled with gravel transport paths indicate that early deposits of petrofacies 3, which contain a tooth of *Neohipparion eurystyle* and therefore predate 4.9 Ma, aggraded in a paleovalley inset into petrofacies 2. We interpret this paleovalley incision, as well as subsequent increased clast caliber and the first appearance of appreciable exotic clasts in petrofacies 3, to reflect an increase in Rio Grande stream power likely related to paleoclimate changes.

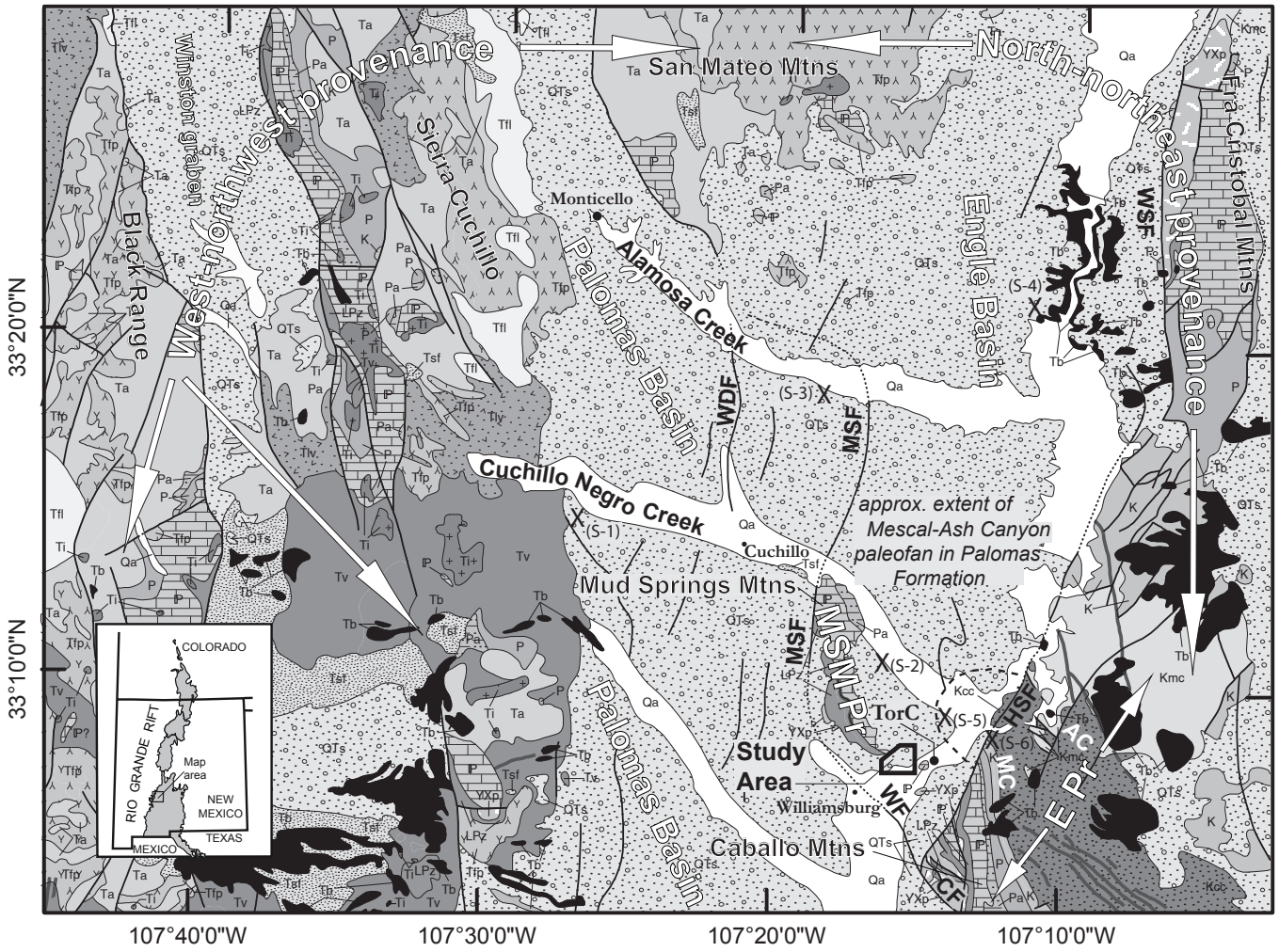
INTRODUCTION

The Rio Grande is an integral feature of the economy, culture, and landscape of New Mexico and the American Southwest. It also serves as the axial river of the Rio Grande rift and flows through the 2016 NMGS Fall Field Conference area in Belen. The geomorphic history of this river relative to the rift has received much study (Denny, 1940; Ruhe, 1962; Kottlowski, 1953, 1958; Kottlowski et al., 1965; Bachman and Mehnert, 1978; Manley, 1979; Baldridge et al., 1980; Smith et al., 2001; Smith, 2004; Connell et al., 2005).

One particularly intriguing event in the history of the Rio Grande rift and its namesake axial river was a remarkable downstream elongation of the Rio Grande from a playa-lake system in the southern Albuquerque and Socorro basins (possibly including the Belen area), where the Rio Grande terminated in the late Miocene, to playa-lakes in the El Paso area (Mack et al., 1997, 2006; Connell, 2004; Connell et al., 2005). This southward expansion resulted in the fluvial integration of several previously closed (endorheic) basins in south-central New Mexico, including the Engle, Palomas, Rincon-Hatch, and Mesilla basins.

Previous studies have only partly constrained the timing of this southward elongation. In the southwestern Socorro basin, stratigraphic relationships coupled with $^{40}Ar/^{39}Ar$ dating of volcanic rocks indicate that the transition between playa lake to through-going axial river occurred between 6.88±0.02 Ma and 3.73±0.1 Ma (respective ages of units Tbsh and Tbsc in Chamberlin and Osburn, 2006, and Chamberlin, 1999, respectively; R.M. Chamberlin, personal commun., 2016). Several independent datasets confirm that the Rio Grande was established in the Engle, Palomas, Hatch-Rincon, and Mesilla basins between 5.0 and 3.0 Ma. Age constraints from associated basin-fill strata include biostratigraphic data (Tedford, 1981; Repenning and May, 1986; Lucas and Oakes, 1986; Morgan and Lucas, 2003, 2011, 2012; Morgan et al., 2011), K/Ar dating of basalts (Bachman and Mehnert, 1978; Seager et al., 1984), $^{40}Ar/^{39}Ar$ dating and intra-basin geochemical correlation of the Hatch Siphon pumice (3.12±0.03 Ma; Mack et al., 1996, 2009) and magnetostratigraphy (Mack et al., 1993, 1998, 2006). Magnetostratigraphic work indicates that the age of earliest Rio Grande deposits in the southern Palomas basin lies between 4.997 and 4.631 Ma (i.e., between the Thvera and Nunivak subchrons, ages per Ogg, 2012). However, the age of earliest Rio Grande deposits in the Engle and northern Palomas basins have not previously been constrained.

This study explores the stratigraphy, provenance, and age of lowest exposed Rio Grande axial deposits within 2 km northwest of downtown Truth or Consequences (T or C) (Fig. 1). There, canyons and a west-east alignment of 5- to 12-m-tall (15- to 40-ft) bluffs display axial-fluvial deposits overlying a scoured contact developed on appreciably finer-grained, redder deposits. A preliminary geologic map of the study area is presented in Figure 2. A useful reference locality in the study area is a prominent quarry owned by BAR-2 Sand and Gravel Inc., located 1 km west of downtown T or C (Fig. 2). This study, combined with on-going investigations, helps elucidate the timing and manner of the arrival of the ancestral Rio Grande into the northern Palomas basin.



EXPLANATION

Middle Pleistocene-Holocene deposits

- Qa — Valley-floor and piedmont alluvium

Miocene-middle Pleistocene basin-fill deposits and basalts

- QTs — Upper Santa Fe Group (includes Palomas Formation)
- Tsf — Lower Santa Fe Group
- Tb — Pliocene basalt flows (rare Miocene flows)

Lower-upper middle Tertiary volcanic and intrusive rocks

- Ti — Intrusive rocks of mostly intermediate composition
- Tv — Volcanic rocks, undivided
- Ta — Basaltic andesites and andesites
- Tfp — Felsic pyroclastic rocks (ash-flow tuffs)
- Tfl — Felsic lavas
- Tlv — Intermediate volcaniclastic sediments with minor intermediate lavas

Cretaceous

- K — Cretaceous rocks, undivided (Gallup Ss through McRae Fm)
- Kmc — McRae Formation
- Kcc — Crevasse Canyon Formation

Paleozoic

- P — Permian rocks, undivided
- Pa — Abo Formation
- IP — Pennsylvanian rocks, undivided
- LPz — Lower Paleozoic rocks, undivided (Cambrian-Mississippian)

Proterozoic

- YXp — Meso- and Paleoproterozoic plutonic rocks, undivided

dike (Ti)

contact

fault; solid where exposed dashed where inferred, dotted where buried.

X(S-#) clast count site (see Table 2; see Fig. 3 for labels in study area).

N

10 5 0 10 km

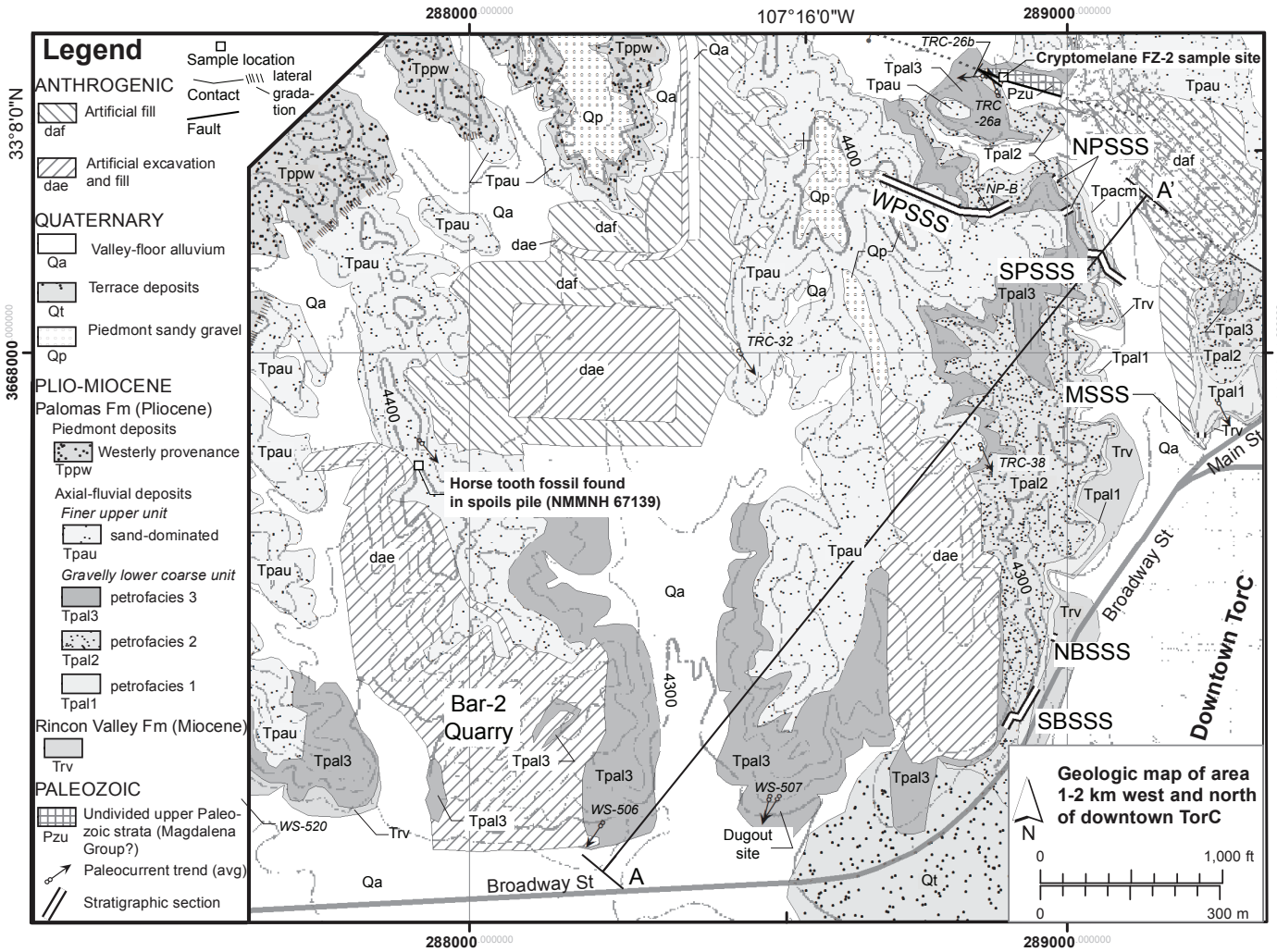


FIGURE 2. Geologic map of the study area (southwest part modified from Jochems and Koning, 2015). Stratigraphic sections are abbreviated as: NBSSS = North Broadway Street, SBSSS = South Broadway Street, MSSS = Main Street, SPSSS = South Poplar Street, NPSSS = North Poplar Street, WPSSS - West Poplar Street. Cross-section A-A' shown in Figure 11.

GEOLOGIC SETTING

The study area (demarcated in Fig. 1) overlies the structural high between the Engle basin to the north and the Palomas basin to the south. This high lies on the footwall of the Mud Springs-Williamsburg faults and includes the Mud Springs Mountains to the northwest of the study area (Fig. 1). Scattered exposures of Proterozoic and Paleozoic bedrock in the downtown area attest to the relative thinness of Rio Grande rift basin fill (i.e., the Santa Fe Group) on this high structural block (Fig. 1). Both the Engle and Palomas basins are east-tilted half-grabens (Lozinsky, 1987; Gilmer et al., 1986). The Engle basin tilts eastward against the Walnut Springs fault (as defined by Machette et al., 1998) at the western base of the Fra Cristobal Mountains, and the Palomas basin tilts eastward towards a fault system at the base of the Caballo and Mud Springs Mountains. This fault system includes the Caballo, Williamsburg, and Muds Springs faults (Seager and Mack, 2003). The Hot Springs fault strikes northeast from the Caballo fault and continues under Elephant Butte Lake towards the southern end of the Walnut Springs fault (Fig. 1).

METHODS

Several procedures were employed in this study. A geologic map (Fig. 2) was constructed using standard field methods (Compton, 1985), a hand-held GPS, and stereogrammetry software (Stereo Analyst for ARCGIS 10.1, an ERDAS extension,

FIGURE 1. Geologic map of the Engle Basin, northern Palomas Basin, and surrounding highlands (modified from NMBGMR, 2003). Annotated faults near Truth of Consequences (TorC) are abbreviated as: CF = Caballo fault, HSF = Hot Springs fault, MSF = Mud Springs fault, WSF = Walnut Springs fault, WF = Williamsburg fault, and WDF = Willow Draw fault. The northern Mud Springs fault coincides with the structural boundary between the overlapping, east-tilted Engle and Palomas basins (Lozinsky, 1987). AC and MC = Ash Canyon and Mescal Canyon, respectively. E Pr and MSM Pr = East Provenance and Mud Springs Mountains provenance regions, respectively (Table 1). The bold box west of T or C demarcates the study area.

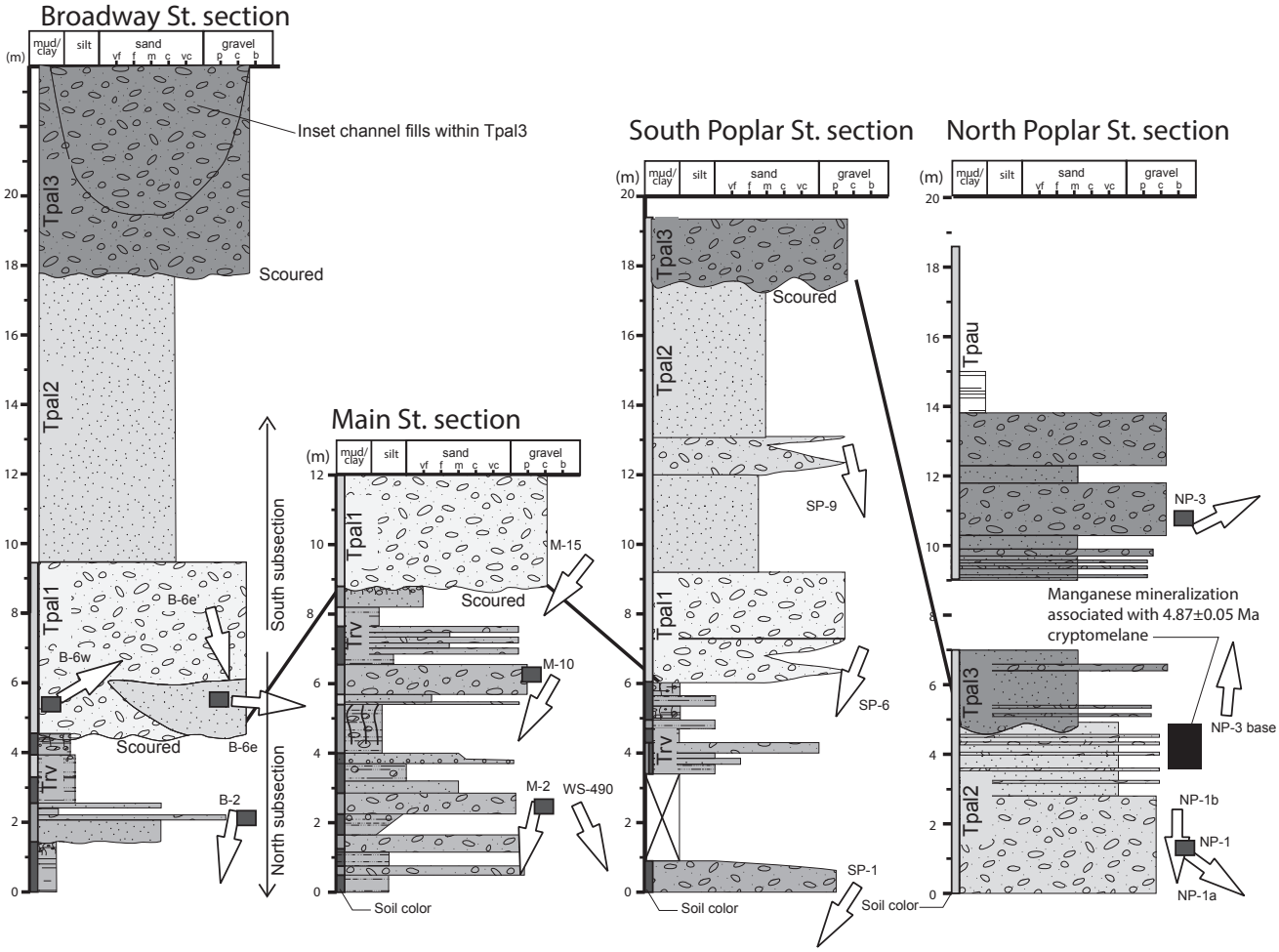


FIGURE 3. Stratigraphic sections illustrating stratigraphic relations of the petrofacies of the lower coarse unit, as well as the scoured contact between the Palomas and Rincon Valley Formations. See Figure 4 for explanation of symbols, shades, and patterns. Annotation of shading follows the map unit nomenclature of Figure 2. Detailed lithologic descriptions provided in Appendix 1.

version 11.0.6). Five stratigraphic sections were measured using an abney level and Jacob staff (Figs. 3, 4); their locations are shown on Figure 2. A horse tooth discovered during geologic mapping was described and measured using the methods outlined in MacFadden (1984).

Twenty-four clast counts were conducted in the field using one of two methods. For weakly consolidated strata, gravel was dug out of a limited area of an outcrop (30- to 50-cm x 30- to 50-cm area), and all clasts >1-cm diameter were identified and tabulated. If strata were cemented, all clasts >1-cm diameter were identified and tabulated on the outcrop face within a specified area (generally 50 x 50 cm). Along stratigraphic sections, clast counts were done on all well-exposed sandy gravels. Outside of the study area, we performed six clast counts of Quaternary gravel deposited by major tributaries between potential source regions and the study area (Fig. 1).

Cryptomelane was dated using the $^{40}Ar/^{39}Ar$ method. While relatively uncommon compared to minerals like sanidine, hornblende, etc., the suitability of using cryptomelane as a mineral phase to be analyzed with the $^{40}Ar/^{39}Ar$ method has been explored by multiple researchers (Vasconcelos, 1999; Lueth et al, 2004). It has been shown to provide reliable age data, if care is taken to prepare a pure mineral separate. A crytotomelane-romanechite sample (FZ-2), collected from brecciated Paleozoic limestones and siltstones in a cemented fault zone, was purified with sieving, handpicking and dilute HCl and HF treatments. The composition of the MnO2 was confirmed by X-ray diffraction. Sample FZ-2 was then analyzed by the $^{40}Ar/^{39}Ar$ method using the incremental, step-heating method.

SEDIMENTOLOGY AND STRATIGRAPHY

Previous Work Near Truth or Consequences Stratigraphy

In the Palomas basin and T or C area, sedimentologic characteristics of lower Rio Grande axial deposits in the Palomas Formation are readily distinguishable from underlying Rincon Valley Formation (as defined by Seager et al., 1971). Specifically, Palomas Formation axial river deposits are coarser-grained than Rincon Valley basin floor deposits, generally contain exotic clasts (described below), and typically feature cross-stratification. Deposits of the Rincon Valley Formation are redder and notably finer-grained (e.g., Koning et al., 2015;

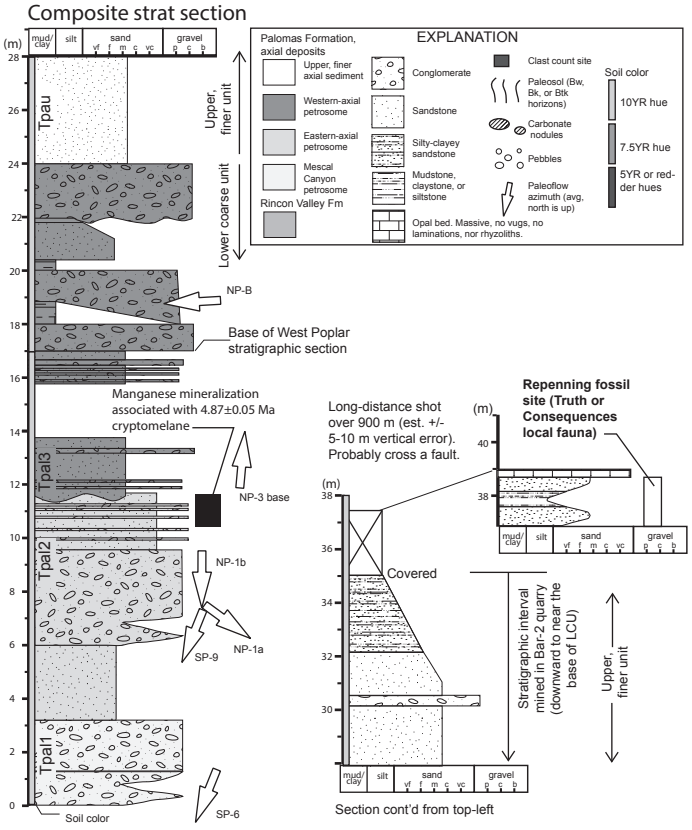


FIGURE 4. Composite stratigraphic section of the South, North, and West North Poplar stratigraphic sections (Fig. 3), including the latter's extension to the Repenning fossil site (~3.3-3.6 Ma; Morgan and Lucas, 2012). Note that the lower 7 m of the composite section corresponds to the 7 m of the South Poplar section overlying the Palomas-Rincon Valley contact, which was correlated to the North Poplar section using the base of petrofacies 3. Annotations of shading follows the map unit nomenclature of Figure 2. Detailed lithologic descriptions provided in Appendix 1.

Jochems and Koning, 2015), with playa deposits being common near basin depocenters (Seager et al., 1971; Mack et al., 1994; Seager and Mack, 2003).

Axial-river Deposits in the T or C Area

Prior to our mapping (Jochems and Koning, 2015), two sets of workers described the stratigraphic and sedimentologic character of ancestral Rio Grande axial-fluvial facies in the T or C area. In the mid-1980s, Richard Lozinsky and John Hawley formally defined the Palomas Formation and differentiated various facies within this formation (Lozinsky and Hawley, 1986a,b; Lozinsky, 1986). Germane to our study is the ≤3-km-wide belt of axial-river facies, which roughly parallels the Hot Springs fault and interfingers to the east and west with piedmont facies of the Palomas Formation. More recently, Foster (2009) and Mack et al. (2012) mapped lithofacies assemblages within the Palomas Formation around the south end of the Mud Springs Mountains, immediately northwest of the study area (Fig. 1). These workers describe the axial-river facies as being cross-stratified sand, with scattered lenses of gravel and clay.

General Stratigraphy

Our study focuses on the lower ~25 m of the axial-fluvial facies of the Palomas Formation, which we note is appreciably coarser than the overlying ~30 m of axial fluvial strata described by previous workers (Lozinsky, 1986; Lozinsky and Hawley, 1986a,b; Foster, 2009; Mack et al., 2012). These overlying strata contain <10% pebbly beds in the T or C area, whereas the lower ~25 m contains 10-50% gravel-bearing strata (Fig. 4). The lower coarse unit (LCU) grades upward into the finer axial deposits. Within the LCU, gravel compositions are used to differentiate three gravel petrofacies that can be mapped (Figs. 2, 5). The axial facies of the Palomas Formation disconformably overlies the redder, fine-grained Rincon Valley Formation. The associated scour has meter-scale vertical relief (Fig. 6). In the underlying Rincon Valley Formation, we designate a western and eastern petrofacies based on gravel composition.

Gravel Source Areas

To determine gravel provenance in our petrofacies units, we designated four generalized highland source areas using the regional distribution of mountains and major drainages (Table 1). In turn, each of the highland source regions can be subdivided into subregions (Table 1). Bedrock lithologies in these source areas were ascertained by clast counts in major drainages in addition to inspecting previous geologic mapping. A fifth gravel source is not a highland area but rather the ancestral Rio Grande transporting gravel into the Engle basin from upstream basins in central and northern New Mexico (Table 1).

The four highland gravel source areas include the Mud Springs Mountains, west-northwest provenance area, north-northeast provenance area, and the eastern provenance area (Fig. 1). The eastern slopes of the Mud Springs Mountains are underlain by Pennsylvanian strata, whose associated detritus is composed predominately of limestone (Table 1). Clast counts from two large creeks draining the west-northwest provenance region, Cuchillo Negro and Alamosa Creek, indicate high abundances of intermediate and felsic volcanic rocks but <10% sedimentary clasts (S-1 thru S-3, Tables 1, 2).

The north-northeast provenance region includes the southeastern San Mateo Mountains, the Fra Cristobal Mountains, and the highlands between the Fra Cristobal Mountains and Ash Canyon (Fig. 1). The southeastern San Mateo Mountains are dominated by felsic tuffs, with very minor amounts of Paleozoic strata and intermediate volcanic rocks (Fig. 1, Table 1). No felsic volcanic rocks are found in the Fra Cristobal Mountains, which are underlain by granite, granitic gneiss, and Paleozoic sedimentary strata (Thompson, 1955; McCleary, 1960; Nelson et al., 2012). Highlands south of the Fra Cristobal Mountains are underlain by sandstones, shales, and minor conglomerates of the McRae and Crevasse Canyon formations (Fig. 1, Table 1). The Love Ranch Formation may have potentially overlain this area in the early Pliocene; if so, erosion of this unit may have contributed gravel composed of Paleozoic

TABLE 1. Inferred gravel characteristics of highland source areas surrounding the Engle and northern Palomas Basins.

Provenance Region	Provenance Subregion	Gravel characteristics*	Method	Clast Count site (Table 2)	Geologic Mapping
Mud Springs Mountains	East flank of Mud Springs Mountains	>90% limestone, trace Abo Fm., 0.5% green siltstone-vf sandstone, variable chert.	Field visits to SCC facies assemblage of Mack et al. (2012)	None	Maxwell and Oakman (1990); Foster (2009)
West-Northwest Provenance	Cuchillo Negro Creek	Intermediate volcanics ≥felsic volcanics; no quartzite or granite; <5% other types (sandstones).	Clast counts and previous mapping	S-1, S-2	Jahns et al. (2006); Harrison and Cikoski (2012); Harrison (1992); Harrison et al. (1986); Cikoski et al. (2012)
	Northern Sierra Cuchillo	Mix of felsic-basaltic volcanics, including felsic tuffs; subordinate Magdalena Group, Abo, Yeso and San Andres Formations.	Previous mapping	None	Maldonado (1980); Heyl et al. (1983); Jahns (1955); Jahns et al. (2006); Harrison et al. (1986); Cikoski et al. (2012)
	Alamosa Creek	Mostly crystal-poor felsic volcanics, ~25% intermediate volcanics.	Clast count and previous mapping	S-3	Koning et al. (2014); Cikoski and Koning (2013); Heyl et al. (1983); McLemore (2010)
	Southwestern San Mateo Mountains	Mix of crystal-poor felsic volcanics and intermediate volcanics; minor Paleozoic strata.	Previous mapping		Foruria (1984); Hermann (1986); Koning et al. (2014)
North-northeast Provenance	Southeastern San Mateo Mountains	Felsic volcanic rocks with very minor amounts of Paleozoic strata and intermediate volcanic rocks.	Previous mapping and clast count	S-4	Furlow (1965); Foruria (1984); Farkas (1969); Osburn (1984); NMBGMR (2003)
	Fra Cristobal Mountains	Granite and granitic gneiss (central part) and Paleozoic strata on southern end.	Previous mapping	None	Thompson (1955), McCleary (1960), Nelson et al. (2012)
	Highlands between Fra Cristobal and Caballo Mountains	Dark brown, green, or purple sandstone; minor gravel dominated by intermediate volcanic gravel; one stratum (≤3 m thick) containing quartzite, gneiss and granite cobbles.	Previous mapping	None	Mason (1976); Lozinsky (1986); Greg Mack (pers. commun., 2016)
Eastern Provenance	Ash Canyon	Greenish-tan-gray, fine- to medium-grained sandstones; local chert and quartz pebbles.	Clast counts and previous mapping. S-5 is from paleofan deposit in Palomas Formation.	S-5	Mason (1976); Lozinsky (1986)
	Mescal Canyon, Northern Caballo Mountains	Limestones and fine- to medium-grained, greenish-tan-gray sandstones.	Clast counts and previous mapping	S-5, S-6	Kelley and Silver (1952); Seager and Mack (2003); Mason (1976)
Rio Grande		Quartzite, chert, felsic volcanic rocks. Pedernal chert clasts observed.	Clast count	S-4	

* Based on clast counts (Table 2) or inferred from geologic mapping.

sedimentary rocks, gneisses, and granites (Seager et al., 1997; Seager and Mack, 2003; W. Seager, personal commun., 2016).

The eastern provenance includes Permian and Cretaceous highlands drained by Ash and Mescal Canyons, the latter of which extends southeast and drains the eastern dip-slopes of the northern Caballo Mountains (Fig. 1). Cretaceous rocks in these drainages generally consist of Crevasse Canyon sandstones; these are mostly fine- to medium-grained and gray, tan, or greenish brown (Table 1; Seager and Mack, 2003). We note that the greenish-grayish Cretaceous sandstones are coarser-grained than greenish-grayish upper Paleozoic sandstones, which tend to be very fine-grained.

To further investigate the eastern provenance region, we closely examined what was mapped as Palomas Formation piedmont facies along the southern slopes of lower Cuchillo Negro Creek (Lozinsky, 1986), southeast of Interstate-25 and 3.5 km northeast of our study area. Well-exposed strata there are in very thin to thin, tabular beds and consist of a light greenish, moderately cemented, pebbly sand and sandy gravel. Measurement of clast imbrication indicates a northwestward

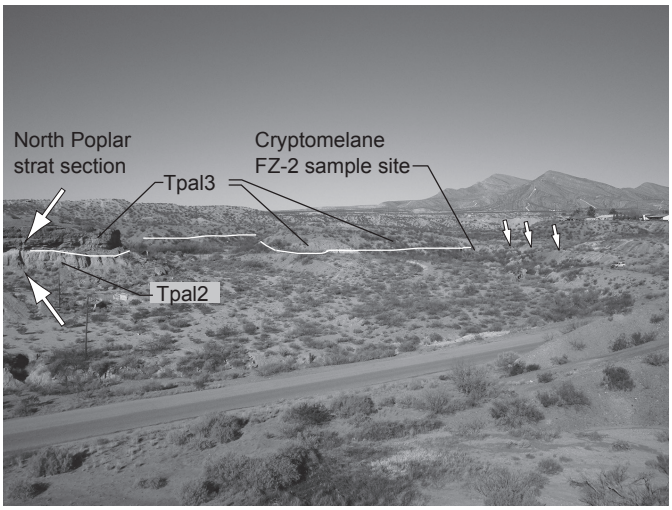


FIGURE 5. Photograph near the cryptomelane FZ-2 sample site illustrating correlation of petrofacies 2 and 3 (labeled Tpal2 and Tpal3, respectively) to the lower 6 m of the North Poplar stratigraphic section (large white arrows). The disconformity between the two petrofacies is illustrated by the white line. View is to the northwest.

component of flow (TRC-7, Appendix 2). The clast assemblage consists wholly of Paleozoic and Mesozoic sedimentary rocks dominated by Paleozoic carbonates, with subordinate sandstones and 8% siltstones and very fine-grained sandstones from the Abo Formation (S-5, Table 2); this gravel composition compares well with a clast count of gravel from the modern-historic floor of Mescal Canyon (S-6, Table 2). The sand fraction is poorly sorted, mostly subangular to subrounded, and consists of about 55-65% quartz, 25-30% lithic grains (of which 2/3 are greenish sandstone and 1/3 are chert or granite), and 15-20% feldspar (estimated using a binocular microscope). This sand exhibits a bimodal color: coarse to very coarse sand is greenish (2.5-5Y 5/2-3) and finer sand is reddish (7.5-10YR 6/6). Across Cuchillo Negro Creek to the north, these strata underlie, and partly interfinger with, Rio Grande fluvial-axial facies. These observations indicate that the light greenish sediment reflects deposition on a paleo-alluvial fan at the mouths of Mescal and Ash Canyons during Palomas Formation deposition. Therefore, this sediment is representative of the eastern provenance region.

We emphasize that quartzite is **not** present in the four highland provenance regions, but quartzite clasts are significant in the Rio Grande point source (Table 2). The only known exception to this assertion is a single, insignificant, ≤3-m-thick stratum of quartzite-bearing conglomerate within the McRae Formation, located south of the Fra Cristobal Mountains in the north-northeastern provenance region (Lozinsky, 1986). Rio Grande gravel is observed at clast count site S-4 (Table 2) in the northern Engle basin (Fig. 1). There, 11% quartzite and 1% Pedernal chert were identified in ca. 3-Ma ancestral Rio Grande strata (Bachman and Mehnert, 1978). In-situ Pedernal chert is restricted to the northwestern Jemez Mountains (Timmer, 1976; Kelley et al., 2013). Based on the absence of bedrock quartzite in the Fra Cristobal and San Mateo Mountains (Table 1), quartzite clasts at S-4 are sourced north of the Engle basin and transported there by the ancestral Rio Grande.

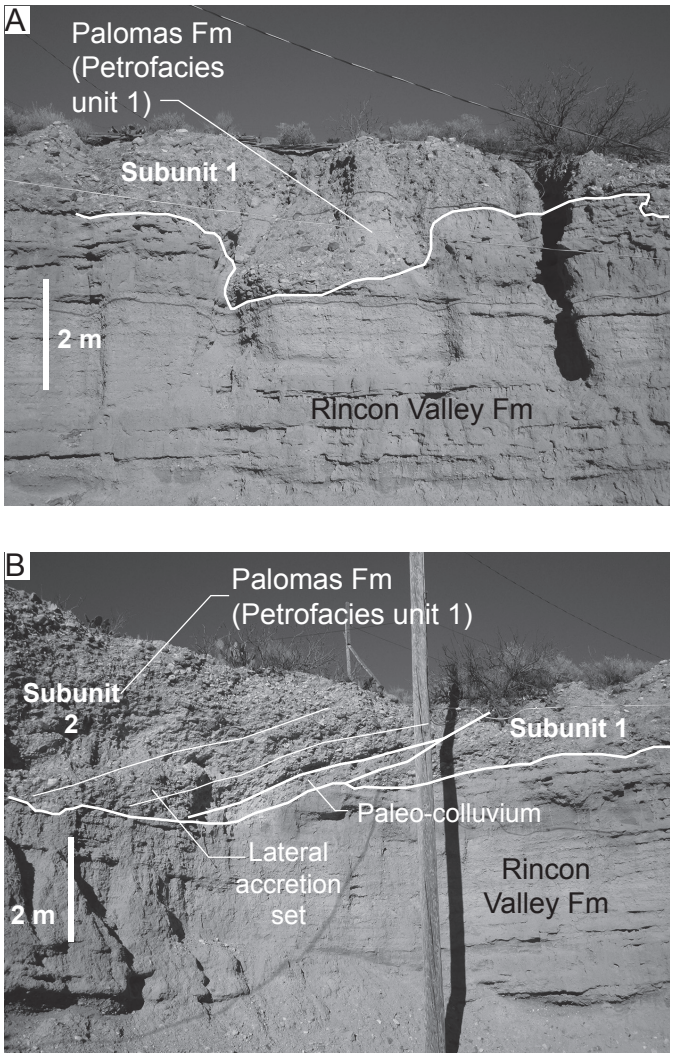


FIGURE 6. Two photographs illustrating the scoured based of the Palomas Formation and inset relationships of gravel in petrofacies unit 1. **A**) Note the 2 m of scour relief generated before aggradation of subunit 1. **B**) After deposition of subunit 1, there was at least 2.5 m of incision followed by aggradation of subunit 2. Note the 2.0- to 2.5-m-thick lateral accretion sets, indicating that paleoflow depth was at least 2 m during deposition of subunit 2. The lateral accretion sets on-lap paleo-colluvium. The presence of paleo-colluvium indicates a period of subaerial exposure.

Lithologic Units North of Downtown

Description

In addition to geologic mapping (Fig. 2), five stratigraphic sections were measured to illustrate lithologic changes (Figs. 3, 4, Appendix 1), listed from south to north: Broadway Street, Main Street, South Poplar Street, North Poplar Street and West Poplar Street stratigraphic sections. The Broadway Street section is comprised of two sub-sections (labeled north and south in Figs. 2, 3). Lithologic units and petrofacies are summarized below. Clast compositions of the various units are tabulated in Table 3, and paleocurrent data are presented in Appendix 2.

The Rincon Valley Formation consists of two relatively fine-grained petrofacies (Fig. 3) that likely interfinger; both exhibit tabular bedding and a reddish color. Locally, calcic paleosols are observed. Both petrofacies contain minor peb-

TABLE 2. Clast count data from deposits reflective of source areas.

Region	West-Northwest Provenance				Northern Provenance	Eastern Provenance	
Subregion	Cuchillo Negro Creek		Alamosa Creek	Average	E San Mateo Mountains and axial Rio Grande	Mescal and Ash Canyons	
Site	S-1	S-2	S-3		S-4	S-5*	S-6
Total felsic volcanic**	10%	47%	72%	60%	55%	0%	0%
Crystal-poor felsic volcanics		31%	50%	41%	39%	0%	0%
Crystal-rich felsitic volcanics		2%	9%	6%	13%	0%	0%
Tuffs, undivided	11%	0%	0%	0%	0%	0%	0%
Kneeling Nun Tuff	3%	14%	0%	7%	0%	0%	0%
Vicks Peak Tuff	0%	0%	13%	7%	3%	0%	0%
Total intermediate volcanics**	48%	42%	26%	34%	15%	0%	0%
Crystal-poor intermediate volcanics		20%	12%	16%	10%	0%	0%
Crystal-rich intermediate volcanics		22%	14%	18%	5%	0%	0%
Paleozoic carbonates	2%	4%	0%	2%	2%	47%	32%
Green vf-f ss and siltstone	0%	0%	0%	0%	0%	23%	30%
Abo Formation	3%	1%	0%	1%	0%	8%	0%
Green, fU-vcU sandstone	0%	0%	0%	0%	0%	7%	21%
Tan siltstone to vf sandstone	0%	3%	0%	2%	0%	5%	0%
Tan, fU-mL sandstone	0%	0%	0%	0%	0%	4%	3%
Total sandstone**	0%	3%	0%	2%	6%	19%	24%
Chert and jasper	1%	0%	0%	0%	3%	2%	4%
Pedernal Chert	0%	0%	0%	0%	1%	0%	0%
Vein quartz	0%	0%	0%	0%	2%	0%	0%
Granite	0%	0%	0%	0%	2%	0%	0%
Quartzite	0%	0%	0%	0%	11%	0%	0%
Basalt	1%	0%	0%	0%	2%	0%	3%
Other	13%	5%	2%	4%	7%	3%	8%
Comments:	Other: 11% intrusive, 2% volcaniclastic sandstone	Other: 1% dacite tuff, 4% intrusive	Other: 1% intrusive and 1% breccia		Other: 2% sandstone, 1 % silicified volcanic, 4% metasandstone	Other: two dark vfL-fL ss, one dark fL-mU quartzose ss	Other: gray, laminated very fine ss to sltst
Easting^	270528	287978	284616		296837	291196	293228
Northing^	3681624	3673353	3687791		3692075	3670830	3669464

* Mescal Canyon paleofan sediment, Palomas Formation on south wall of Cuchillo Negro Creek east of I-25.
** Includes relevant clast types in "other" category; felsic and intermediate volcanics not differentiated in S-1.
^ Coordinates are UTM in meters; datum is NAD83 (zone 13).
Sand-grain sizes follow the Udden-Wentworth scale for clastic sediments (Udden, 1914; Wentworth, 1922): vfL = very fine lower, fL = fine lower, fU = fine upper, mL = medium lower, mU = medium upper, vcU = very coarse upper. Ss = sandstone, sltst = siltstone.

TABLE 3. Clast count data from Pliocene sedimentary deposits in study area.

Site*:	WS520	TRC24	M-2	M-10	B-2	SP-1	M-15	B-6w	SP-6	B-6e	NP-1	TRC-26a	NP-3	NP-3AJ	WS506	WS507	TRC-26b	WP-B
Petrofacies:	**Trvw****	**Trvw**	**Trve**	**Trve**	**Trve**	**Trve**	**Tpa1**	**Tpa1**	**Tpa1**	**Tpa2**	**Tpa2**	**Tpa2**	**Tpa3**	**Tpa3**	**Tpa3**	**Tpa3**	**Tpa3**	**Tpa3**
Vein quartz	0%	0%	2%	0%	1%	0%	0%	1%	0%	1%	0%	0%	0%	0%	0%	1%	1%	0%
Proterozoic gneiss	5%	0%	7%	1%	9%	9%	0%	1%	2%	0%	2%	1%	0%	0%	2%	1%	3%	6%
Chert	25%	0%	17%	5%	0%	5%	0%	2%	0%	0%	2%	3%	0%	2%	5%	7%	5%	4%
Undivided felsic volc.§	60%	53%	0%	1%	1%	2%	2%	1%	4%	82%	53%	57%	37%	37%	21%	12%	30%	21%
Felsic tuff	4%	30%	0%	0%	0%	0%	0%	0%	0%	0%	26%	9%	21%	2%	8%	1%	--	--
Intermediate volcanics		7%	0%	0%	0%	5%	0%	0%	9%	0%	2%	1%	21%	25%	24%	19%	26%	27%
Paleozoic carbonates		0%	52%	42%	37%	56%	66%	83%	35%	7%	0%	6%	6%	9%	0%	0%	6%	19%
Green vf-f ss and sltst		0%	5%	1%	2%	0%	0%	2%	4%	0%	0%	3%	0%	1%	1%	0%	0%	0%
Qtzose sandstone***		0%	2%	0%	1%	0%	0%	0%	0%	0%	0%	2%	0%	4%	1%	1%	2%	0%
Green K sandstone		4%	6%	36%	8%	7%	29%	5%	25%	8%	8%	7%	0%	0%	1%	1%	5%	0%
Granite	5%	1%	6%	0%	20%	0%	0%	1%	0%	0%	7%	5%	1%	4%	6%	7%	0%	0%
Abo Fm		1%	5%	14%	19%	12%	3%	5%	21%	2%	1%	2%	0%	0%	2%	0%	2%	0%
Quartzite		0%	0%	0%	0%	0%	0%	0%	0%	0%	0%	0%	10%	12%	20%	43%	17%	17%
Basalt		0%	0%	0%	0%	0%	0%	0%	0%	0%	0%	0%	3%	0%	1%	3%	0%	0%
Other		4%	0%	0%	0%	0%	0	0%	0%	0%	0%	4%	0%	2%	6%	1%	3%	1%
Comments:		Other: Tertiary ss and 1 un-ID										Other: 1 volc ss, 3 intra-fm ss		Other: non-granite intrusive	Other: Un-identified	Ortega quartzite(?) and other un-ID		3 Ortega quartzite(?) Pedernal chert - 1%
Easting^	287552	289442	289224	289219	288977	289066	289222	288974	289041		288985	288849	288997	289000	288204	288502	288844	288880
Northing^	3667305	3668059	3667860	3667865	3667526	3668141	3667868	3667533	3668168	3667536	3668291	3668465	3668237	3668227	3667195	3667239	3668469	3668235

Notes:

* Sites prefixed by WS or TRC are labeled on geologic map (Fig. 2). Other prefixes denote sites in stratigraphic sections: NP = North Poplar, SP = South Poplar, M = Main Street, B = Broadway.

** Based on visual estimation.

*** Locally a metasandstone.

§ Category does not include the recognized tuffs differentiated in the next row.

^ UTM coordinates are in meters; datum is NAD83 (zone 13).

"--" Not differentiated and subsumed into "undivided felsic volcanics."

Petrofacies nomenclature follows that in Figure 2, except that the Rincon Valley Formation is subdivided into an eastern and western petrofacies (see manuscript text).

un-ID = unidentified.

K = Cretaceous, volc = volcanic, slst = siltstone, ss = sandstone, vf-f = very fine to fine grained.

ble beds composed of subangular clasts. The western Rincon Valley petrofacies (Trvw, Table 3) is dominated by clasts of felsic volcanic rocks, but the eastern Rincon Valley petrofacies (Trve, Table 3) contains mostly sedimentary clasts (i.e., Paleozoic limestone, red siltstone-very fine sandstone of the Abo Formation, greenish fine- to medium-grained Cretaceous sandstones). Minor granite, chert, and gneissic clasts are also present (Table 3). Paleoflow directions are 150-215° (Fig. 3, Appendix 2). Sand in the Rincon Valley Formation is reddish (7.5-5YR hues), angular to subrounded, and has relatively low amounts of quartz (generally % feldspar + % lithic grains is greater than % quartz grains).

Strata of the lower coarse unit (LCU) of the axial-fluvial Palomas Formation are notably coarser and grayer than the aforementioned Rincon Valley Formation (Fig 3; Appendix 1). Clast sizes are also significantly larger (Fig. 7). Floodplain deposits are practically absent in the lower ~15 m of the LCU, but are more abundant above (Fig. 4). Cross-stratification sets are typically 0.1 to 1.0 m thick. Planar foresets commonly dip transverse to flow direction, indicating lateral accretion sets (Figs. 6, 8). Sand is generally very pale brown to white (10YR hues), commonly horizontal-planar laminated, medium- to very coarse-grained, subangular to well-rounded, and generally quartz-rich (i.e., % quartz is greater than % feldspar + lithics). Paleosols are very sparse in the axial-fluvial sediment, with only a weak Bw horizon seen at one locality (Fig. 8).

We recognize three petrofacies in the LCU containing unique gravel compositions and gravel sizes (Tables 3, 4; Figures 3, 4, 7-10). The sand fraction of the three petrofacies is broadly consistent with that described above for the LCU. Gravel in petrofacies 1 is composed chiefly of Paleozoic carbonate rocks (35-90%) with minor (3-20%) Abo Formation siltstones and very fine-grained sandstones; quartzite is absent. Petrofacies 2 also lacks quartzite clasts and is composed predominately of felsic volcanic types; Paleozoic-Mesozoic sedimentary clasts are minor (10-20%), and intermediate volcanic clasts are very minor (0-2%). Petrofacies 3 is comprised predominately of intermediate and felsic clasts with 10-40% quartzite and 0-10% chert.

Stratigraphic Relationships

Stratigraphic relationships between the Palomas axial petrofacies elucidate the depositional history of the LCU (Fig. 11). Petrofacies 1 occupies the basal 3-5 m of the LCU in the eastern part of the study area. Higher in the section, petrofacies 3 overlies petrofacies 2 in the eastern study area, and the associated contact is highly scoured (Fig. 9). Notably, interfingering relationships between the petrofacies is limited, with no interfingering observed between petrofacies units 2 and 3. There are minor interbeds of petrofacies 2 within the western part of petrofacies 1 (e.g., Fig. 3, Broadway stratigraphic section; Fig. 8) as well as minor interbeds of petrofacies 1 within the eastern part of petrofacies 2.

Stratigraphic inset relations can be observed within petrofacies 1. At one locality immediately north of downtown, slightly(?) younger fluvial gravels can be observed inset into older fluvial gravels (Fig. 6). A thin layer of colluvium overlies at least part of the buttress, but it has no obvious soil development. Overlying the colluvium are 2.0-2.5 m-thick lateral accretion foresets of the younger fluvial gravel (subunit 2, Fig. 6).

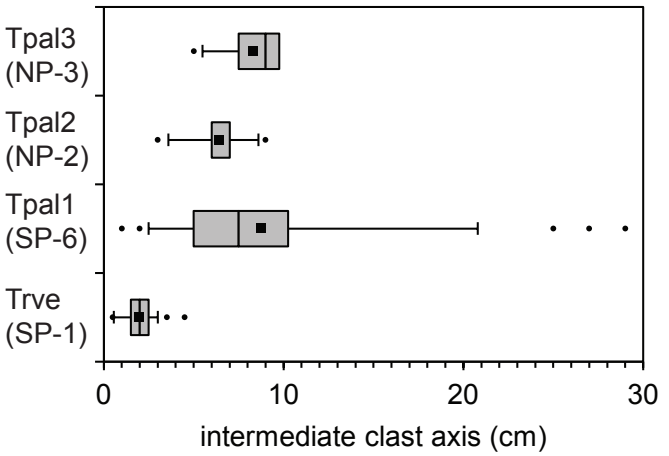


FIGURE 7. Box-and-whisker plot comparing maximum clast sizes between the eastern petrofacies of the Rincon Valley Formation (Trve) and the three petrofacies of the lower coarse unit of the Palomas Formation (Tpa1, Tpa2, Tpa3). Measurements were taken from the North Poplar (NP) and South Poplar (SP) stratigraphic sections (Appendix 1).



FIGURE 8. Photograph of petrofacies unit 1 exhibiting of thin to medium, tabular to lenticular beds of sandy gravel. Planar foresets of a ~0.8-m-thick lateral accretion set are annotated by the white lines. Gravel is composed of Mesozoic and Paleozoic sedimentary clasts. Large arrow denotes interbed of petrofacies unit 2 that is comprised of clean sand containing felsic volcanic pebbles. Clast imbrications indicate southerly paleoflow. Squiggly black lines in upper right of photo indicate location of a weak Bw horizon of a paleosol. Rock hammer for scale (small arrow). Site is located 175 m west-southwest of the Main Street stratigraphic section.

AGE CONTROL

Neohipparion eurystyle Tooth From the Palomas Formation

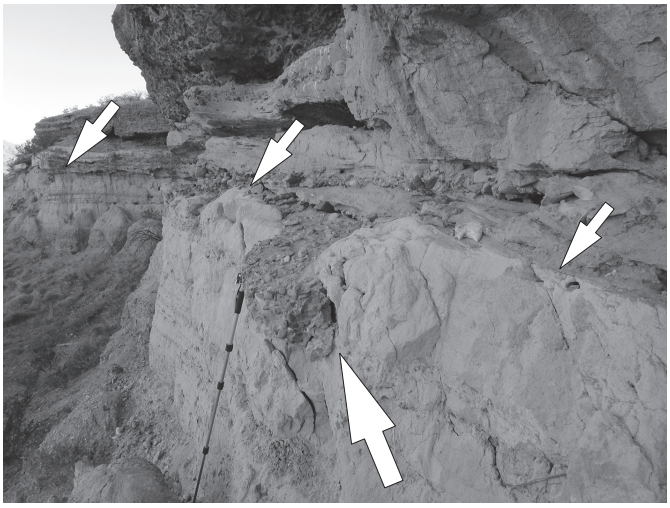
Location

A fossil horse tooth was collected from a spoil pile at the northern boundary of the BAR-2 Quarry (Figs. 2, 12), at UTM

TABLE 4. Summary of lower coarse unit petrofacies (Palomas Formation).

Petrofacies	Major clasts	Minor clasts	Texture/ gravel sizes	Other	Paleoflow	Provenance
Petrofacies 1	Pz carbonates (35-90%).	Green K sandstones (5-30%); Abo Formation (3-20%); 0-2% chert; 0-2% granite and gneiss; 1-5% felsic volcanics.	Sandy conglomerate. Subequal cobbles and pebbles, 0-20% boulders.	Lenses of petrofacies 2 more common to west (e.g. Broadway stratigraphic section). Clasts are subangular to rounded and very poorly sorted.	193-202° Broadway stratigraphic section: 59° and165°.	East, minor north-northeast.
Petrofacies 2	Felsic volcanic rocks.	0-10% gneiss and granite; 0-2% intermediate volcanics; 0-3% chert; 1-10% Pz sedimentary, 5-10% K sandstones.	Sand with subequal pebble-cobbles.	More sandy than petrofacies 1; gravel are angular to rounded and poorly sorted.	151°-167°	North-northeast.
Petrofacies 3	10-60% felsic and 20-30% intermediate volcanic clasts, generally about subequal. 10-40% exotic quartzite.	<20% Pz carbonates; <10% granite. ≤5% (each) of greenish sandstones-siltstones, quartzose sandstones, basalt, and Abo Formation clasts. 0-10% chert (trace Pedernal chert).	Interbedded sand and gravel. Gravel has abundant cobbles.	Exotic clasts include Pedernal chert and abundant quartzite. Quartzite include cross-laminated varieties inferred to correlate to Ortega Quartzite.	Variable, ranging from NE to SE to SW.	West-northwest and north-northeast.

Notes:
Pz = Paleozoic; K = Cretaceous.



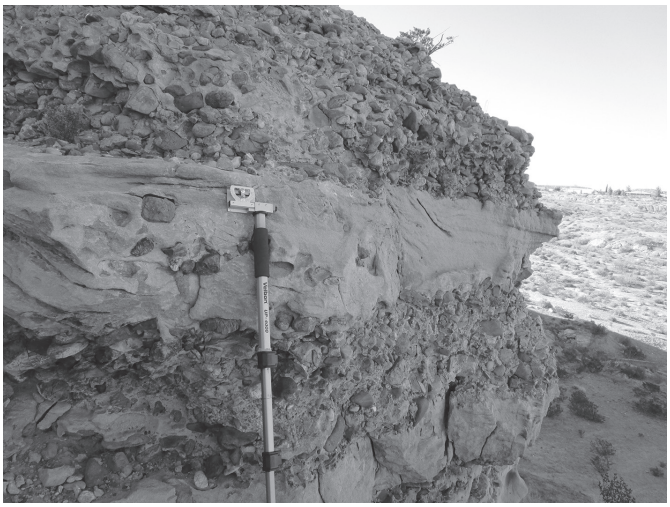


FIGURE 9. Annotated photographs of petrofacies units 2 and 3 at the North Poplar stratigraphic section. Small arrows denote the contact between petrofacies 3 (above) and petrofacies 2 (below). This contact is highly scoured and coincides with a disconformity. One particularly large scour groove is shown by the large arrow in the top photograph. The bottom photograph shows a close-up of the middle part of petrofacies unit 3, where clast count site NPSS-3 is located; abney level for scale. Note the strong cementation of petrofacies unit 3 at this locality, although in most places it is weakly cemented.

coordinates 287,905 m E, 3,667,827 m N (NAD 83, zone 13). Excavations and disturbance associated with the quarry extends from 4280 to 4400 ft in elevation (Figs. 2, 11), and the tooth-bearing spoil pile is at the top of this disturbance. The gravel in the spoil pile consists of felsite volcanic clasts with 20-30% intermediate volcanic clasts, 3% basaltic andesite, 1% granite, 3% chert, 2% quartzite, and trace Abo Formation (visual estimation). The high proportion of intermediate clasts and the presence of exotic quartzite clasts strongly suggest the tooth came from petrofacies 3 of the LCU, which is restricted to the lower-middle part of the quarry (Fig. 11). Unfortunately, the owner of the quarry did not provide specific information regarding the source of the sediment in the spoil pile.

Description

The collected horse tooth (catalog number NMMNH 67139) consists of the labial half of a right upper molar, either the first molar (M1) or second molar (M2). The lingual half of the tooth with the protocone is missing (Fig. 12). In labial view, the tooth is noticeably curved posteriorly, especially the distal half of the tooth just above the root, suggesting that this probably represents an M2 (Fig. 12). The M1 of most hipparionine horses tends to be vertical or only slightly curved posteriorly. On the anterolabial margin of the tooth, there is a strong parastyle with a definite posterior curvature labially. The mesostyle is noticeably "pinched" at its base, whereas the labialmost extension of the mesostyle is noticeably curved anteriorly. The metastyle is broken, so it is not possible to determine its orientation. The two fossettes located just lingual to the ectoloph have fairly complicated enamel. The fossettes have a total of nine plica-

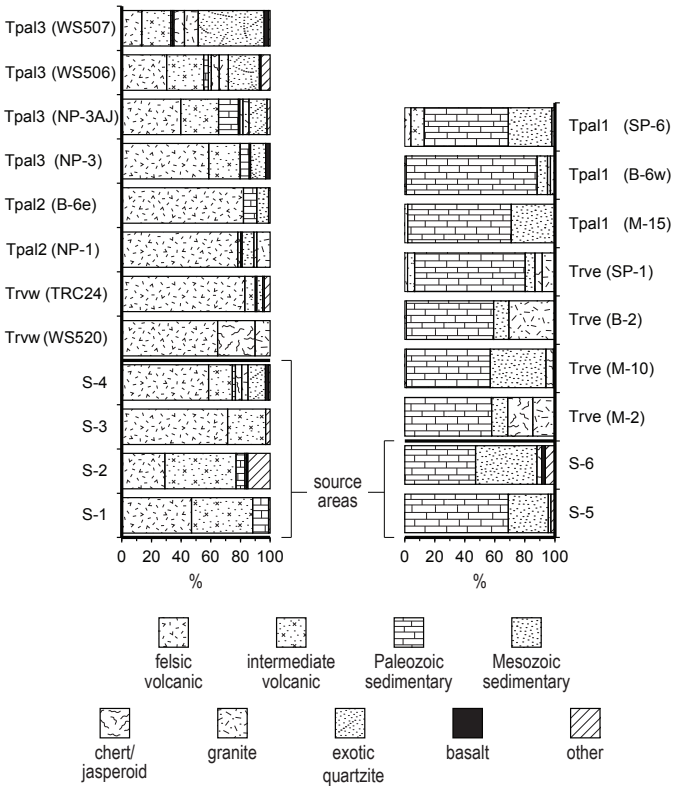


FIGURE 10. Bar graphs illustrating gravel composition at various clast count sites. Gravel data on the right column are comprised predominately of sedimentary clasts derived from the eastern provenance region. To the side of a given bar is the associated petrofacies (labels follow those on Fig. 2) and site name (in parentheses). Sites are labeled on Figure 2 (for those prefixed by "WS" or "TRC") or else are associated with stratigraphic sections (Figs 3, 4; Appendix 1). Stratigraphic section abbreviations: NP = North Poplar; SP = South Poplar; M = Main Street; B= Broadway Street. Not all sites listed in Table 3 are illustrated on this figure. Source area sites are located on Figure 1.

tions: one plication on the anterior half of the prefossette, five on the posterior half of the prefossete, and three on the anterior half of the postfossette. The posterior margin of the postfossette lacks enamel plications.

Measurements of NMMNH 67139 are anteroposterior length, from protoloph to posteriormost enamel on tooth (excluding ectoloph), 21.7 mm; anteroposterior length of ectoloph, from parastyle to metastyle, 22.2 mm; mesostyle crown height, 61.2 mm. All measurements were taken on enamel; cementum is excluded.

Comparisons

The NMMNH 67139 partial horse tooth (M1/M2; NMMNH 67139) is most similar to upper molars of the three-toed or hipparionine horse *Neohipparion eurystyle*, so we tentatively identify NMMNH 67139 as that species. The anteroposterior length of the tooth (21.7 mm) is within the observed range of this measurement for the M1 in *N. eurystyle* (observed range 19.3-24.4 mm, mean 21.2 mm; comparative measurements from MacFadden, 1984). In addition to size, NMMNH 67139 and *N. eurystyle* are similar in the enamel complication of the fossettes (nine total plications in NMMNH 67139; observed range of 8-14 plications for *N. eurystyle*, mean of 10 plications; from MacFadden, 1984). The absence of an enamel plication along the posterior margin of the postfossette in the NMMNH 67139 tooth differs from most upper molars of *N. eurystyle*, which generally have a single enamel plication on the posterior half of the postfossette. However, this characteristic is somewhat variable, and some upper molars of *N. eurystyle* lack this enamel plication. The NMMNH 67139 tooth has a fairly strong, posteriorly curved parastyle that is similar to that of *N. eurystyle*. The parastyle in NMMNH 67139 is somewhat weaker than expected in a *N. eurystyle* upper but is probably within the range of individual variation in the species. The base of the mesostyle is strongly pinched, while the labial portion of the mesostyle is strongly curved anteriorly.

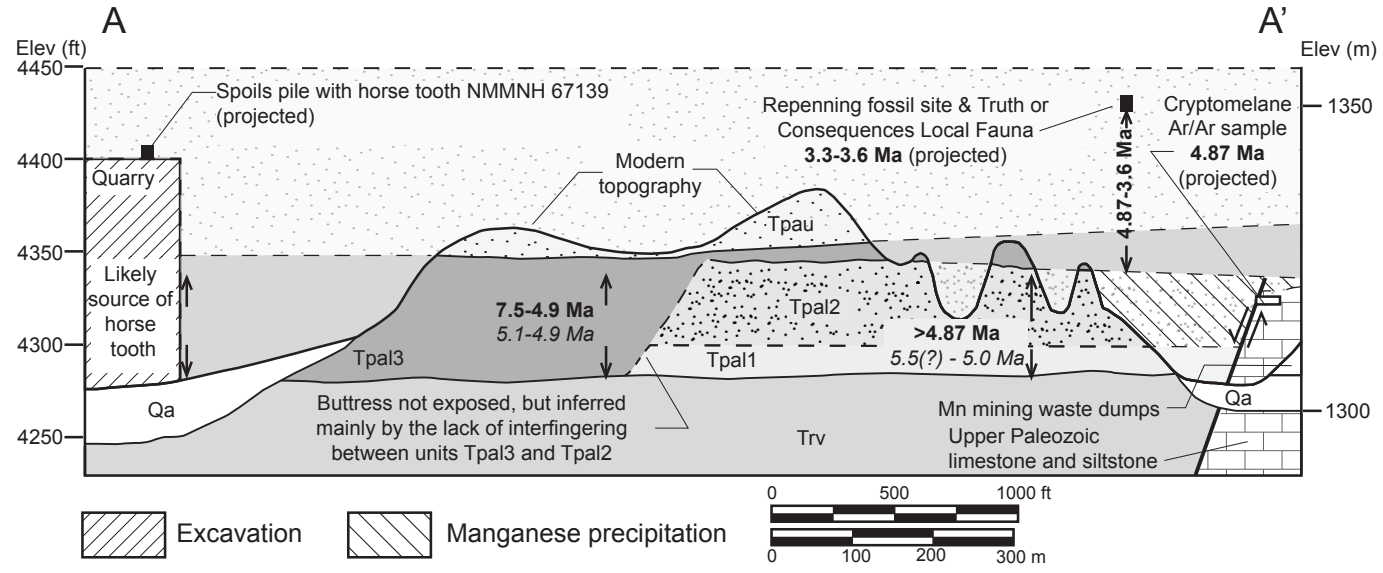


FIGURE 11. Stratigraphic relationships of the petrofacies units in the study area, as illustrated by a cross-section drawn along A-A' in Figure 2. Contact elevations are projected horizontally onto the line of section from exposures within 400 m of the cross-section line. Lithologic unit abbreviations follow those in Figure 2. Bold ages are strictly based on biostratigraphic or $^{40}Ar/^{39}Ar$ constraints; non-bold ages are inferred.

The "pinched" mesostyle is characteristic of *N. eurystyle* and *N. gidleyi*. A large, anteriorly curved metastyle is a characteristic feature of *N. eurystyle*. Because the metastyle is damaged in the NMMNH 67139 tooth, it is not possible to determine its size or orientation. The NMMNH 67139 tooth agrees with the upper molars of *N. eurystyle* in being fairly straight in anterior or posterior view; it is not strongly curved as in many other genera of late Miocene horses. Another species of *Neohipparion*, *N. gidleyi*, is known from the late Hemphillian of New Mexico but is noticeably larger than the NMMNH 67139 tooth in anteroposterior length (measurements from MacFadden, 1984).

Because NMMNH 67139 is incomplete, it is important to briefly discuss characteristics that distinguish it from other horse upper molars known from New Mexico Hemphillian and Blancan faunas. Based on its size, the tooth is too small for *Equus* and too large for *Nannippus*, which excludes the two genera of horses known from New Mexico Blancan faunas (Pliocene and early Pleistocene). Three species of horses are known from latest Hemphillian faunas in New Mexico: *Astrohippus stockii*, *Dinohippus mexicanus*, and *Neohipparion eurystyle* (Morgan et al., 1997; Morgan, 2015). NMMNH 67139 is larger than *A. stockii* and smaller than *D. mexicanus* and has more complicated fossettes than either of those species. Most upper molars of *A. stockii* and *D. mexicanus* have no enamel plications in the fossettes or at most one plication, whereas the NMMNH 67139 tooth has nine enamel plications. A single lower molar of *Neohipparion eurystyle* was identified from the Glenwood fauna (Morgan, 2015). Although this specimen is not directly comparable to the upper molar of NMMNH 67139, both specimens are very similar to teeth of *N. eurystyle* from the latest Hemphillian Palmetto Faunas in Florida (MacFadden, 1984; Hulbert, 1987).

Biochronologic range

Neohipparion eurystyle had a fairly long biochronologic range during the late Miocene and early Pliocene, first appearing in the late early Hemphillian (~7.5 Ma) and becoming extinct at the end of the Hemphillian (~4.9 Ma), together with several other genera of horses (MacFadden, 1984; Hulbert, 1987). The latest Hemphillian Glenwood fauna from the Gila region of southwestern New Mexico is one of the youngest well-dated records of *N. eurystyle* (Morgan et al., 1997; Morgan, 2015). The age of the Glenwood fauna is restricted to between 5.6 and 4.9 Ma, based on a latest Miocene date of 5.6 ± 0.3 Ma on the Harve Gulch basalt underlying the fauna (Ratté and Finnell, 1978; Houser, 1987) and the presence of Blancan (younger than 4.9 Ma) vertebrates from Gila Group strata overlying this fauna in the Mangas basin, specifically the early Blancan Buckhorn fauna (Morgan et al., 1997; Morgan, 2015).

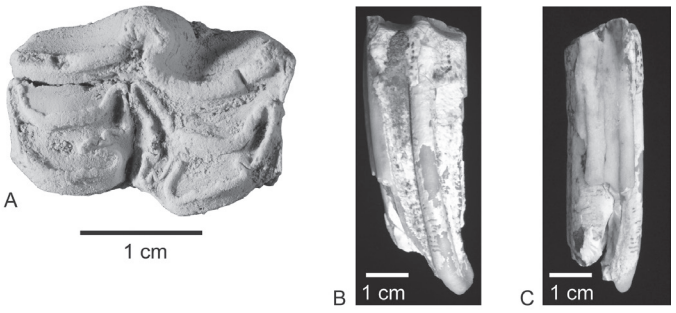


FIGURE 12. Partial upper molar (M1 or M2) of *Neohipparion eurystyle* (Equidae) collected from a spoil pile at the top of the Bar-2 quarry site (NMMNH 67139, NMMNH locality L-8699). This species is part of the late Hemphillian North American land-mammal "age" (~7.5 to 4.9 Ma). **A**) Occlusal view (Tooth whitened with ammonium chloride in photograph), **B**) Labial view, **C**) Anterior view.

Cryptomelane Occurrence and $^{40}Ar/^{39}Ar$ Results

Location and Stratigraphic Relationships

Cryptomelane from a fault zone was initially sampled (sample FZ-2) to determine the age and duration of hot spring development in the T or C geothermal area (Fig. 13). This fault is within altered limestones and siltstones correlated to the Pennsylvanian-age Magdalena Group by Lozinsky (1986). The larger fault zone is several meters wide and includes faults within upper Paleozoic strata as well as a southwest-down normal fault juxtaposing petrofacies 2 on the hanging wall against altered upper Paleozoic strata on the footwall (southern fault strand in Fig. 13A, B). Petrofacies 3 extends over this southern fault strand (Fig. 13A), but fault-related tilting and offset occurred after its deposition. Within the hanging wall, manganese mineralization has occurred in petrofacies 2, and carbonate clasts are altered and partially dissolved. Where it overlies the fault zone, petrofacies 2 is well-cemented by calcium carbonate and cryptomelane (Fig. 13D). Mineralogy, petrology, and occurrences of additional manganese oxide deposits in the Palomas Formation are presented in Lueth (2012).

The scoured contact between the western and petrofacies 2 can be easily traced from the cryptomelane sample site to the North Poplar stratigraphic section (Fig. 5). At the cryptomelane sample site, the overlying petrofacies 3 has no manganese cementation and is only locally cemented by calcium carbonate (Figs. 11, 13C). These relationships indicate that the highly scoured contact between the two petrofacies is a disconformity.

$^{40}Ar/^{39}Ar$ Results

Sample FZ-2 yielded a well-behaved, nearly flat age spectrum (Fig. 14, Appendix 3). Over 96% of the ^{39}Ar released was used to calculate a weighted mean age 4.87±0.05 Ma. The data was evaluated with the inverse isochron technique and found to have a nearly atmospheric intercept of 294.5±0.7 and an isochron age of 4.92±0.06 Ma, within error of the weighted mean age assigned to the age spectrum. We have assigned the weighted mean age calculated from steps G-L of the age spectrum (4.87±0.05 Ma) as the preferred age for the formation of this cryptomelane.

DISCUSSION

Source Areas of Petrofacies

The Rincon Valley Formation lacks prominent cross-stratification and extra-basinal clasts, and its sand fraction is relatively angular and quartz-poor. The predominance of felsic volcanic clasts in the Rincon Valley western petrofacies — together

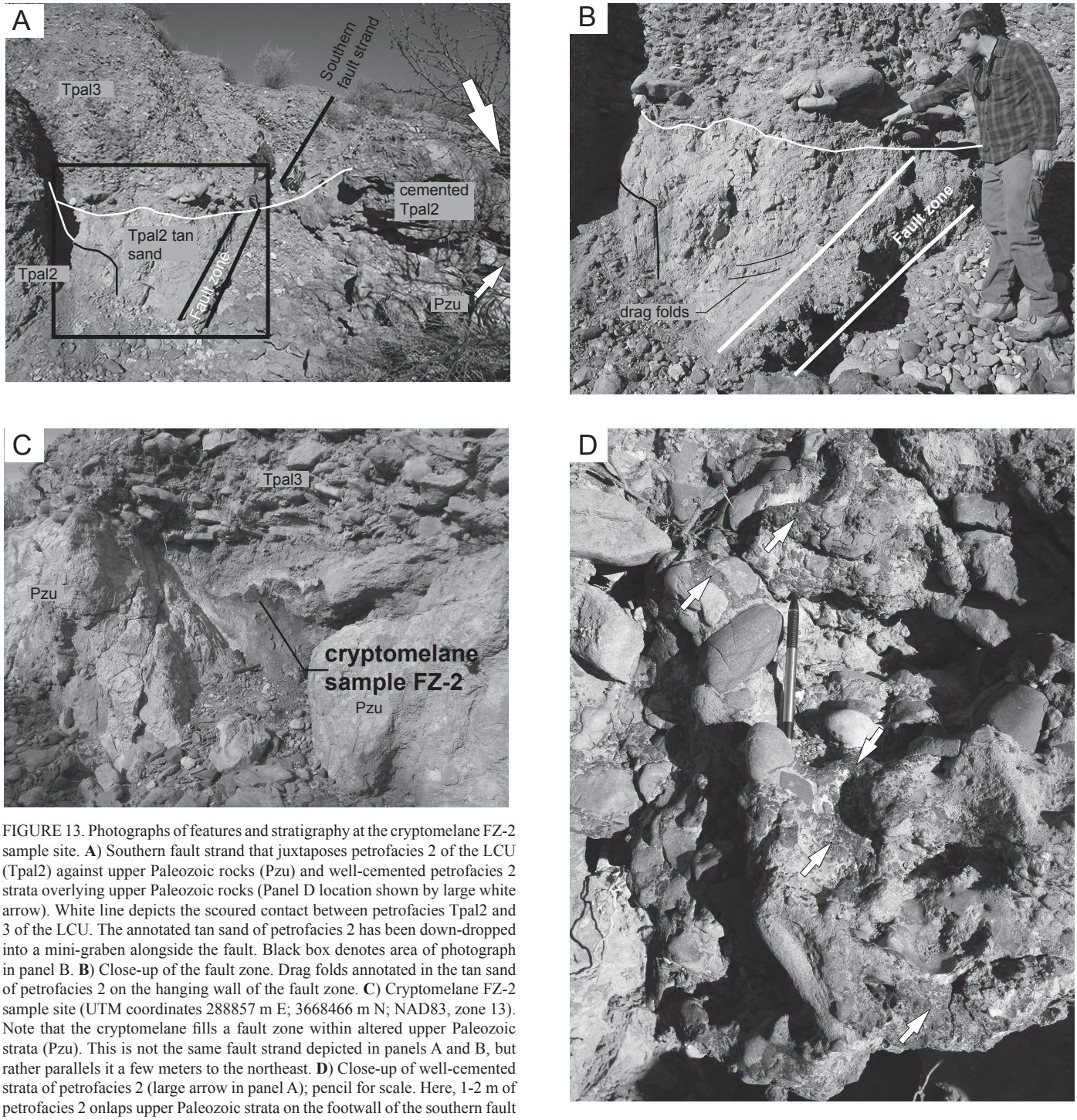


FIGURE 13. Photographs of features and stratigraphy at the cryptomelane FZ-2 sample site. **A**) Southern fault strand that juxtaposes petrofacies 2 of the LCU (Tpal2) against upper Paleozoic rocks (Pzu) and well-cemented petrofacies 2 strata overlying upper Paleozoic rocks (Panel D location shown by large white arrow). White line depicts the scoured contact between petrofacies Tpal2 and 3 of the LCU. The annotated tan sand of petrofacies 2 has been down-dropped into a mini-graben alongside the fault. Black box denotes area of photograph in panel B. **B**) Close-up of the fault zone. Drag folds annotated in the tan sand of petrofacies 2 on the hanging wall of the fault zone. **C**) Cryptomelane FZ-2 sample site (UTM coordinates 288857 m E; 3668466 m N; NAD83, zone 13). Note that the cryptomelane fills a fault zone within altered upper Paleozoic strata (Pzu). This is not the same fault strand depicted in panels A and B, but rather parallels it a few meters to the northeast. **D**) Close-up of well-cemented strata of petrofacies 2 (large arrow in panel A); pencil for scale. Here, 1-2 m of petrofacies 2 onlaps upper Paleozoic strata on the footwall of the southern fault strand. Small white arrows show the black cryptomelane cement.

with minor granite, gneiss, and green Cretaceous sandstones (Table 3) — is supportive of a north-northeast provenance region. Southerly paleocurrents measured in the Rincon Valley western petrofacies are consistent with the general south-southwest paleocurrent directions measured in the Rincon Valley eastern petrofacies at our stratigraphic sections (Fig. 3). This means that drainages flowed southward through the study area during deposition of exposed Rincon Valley strata, connecting the southern Engle basin with the northern Palomas basin.

Previous workers have made no attempts to reconstruct the paleogeography of the Engle basin during the latest Miocene. However, that the Engle basin existed throughout most or all of post-Oligocene Rio Grande rifting is reasonable considering that: (1) a prominent gravity low coincides with the current basin, with a steeper eastern flank than western flank consistent with an east-tilted half-graben (Gilmer et al., 1986) and that (2) the basin fill in the southern part of the basin is estimated to be ~700 m thick (Lozinsky, 1987). The latter thickness measure-

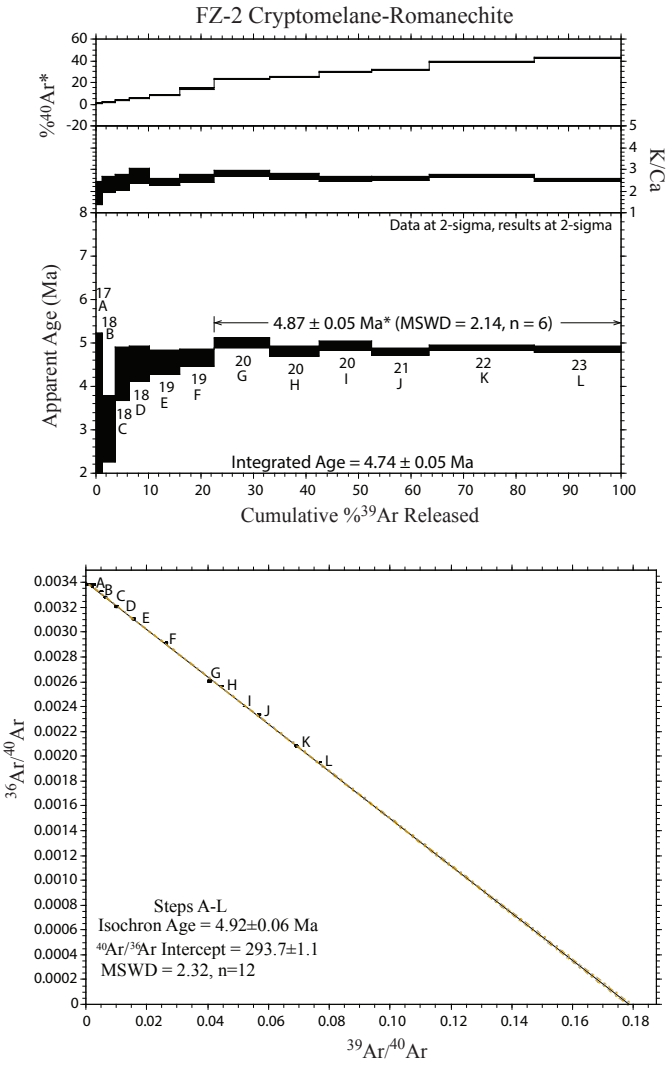


FIGURE 14. $^{40}Ar/^{39}Ar$ spectra and inverse isochron plots for sample FZ-2, the cryptomelane sample collected from the fault mapped in the northeast study area. Associated data table is in Appendix 3.

ment is 16 km south of the lowest Bouguer anomaly values and thus likely underrepresents the maximum basin-fill thickness. Even so, the ~700-m basin-fill thickness is twice as thick as the 240-300 m maximum thickness of the Plio-Pleistocene Palomas Formation in the Palomas basin (Koning et al., 2015; Jochems and Koning, 2015), and this strongly implies that the Engle basin subsided during the Miocene and Plio-Pleistocene.

The Rincon Valley eastern petrofacies has abundant Paleozoic and Mesozoic sedimentary clasts consistent with an eastern provenance region, but the presence of 1-30% Proterozoic rocks (gneiss and granite) and 0-2% felsic volcanic rocks indicate minor secondary contributions from the north-northeast provenance region. Based on its general south-southwesterly paleocurrents and tabular-bedded sedimentary architecture, the Rincon Valley eastern petrofacies is interpreted to reflect deposition on a distalmost piedmont by drainages primarily sourced in the eastern provenance region.

In the LCU of the Palomas Formation, the coarse texture, bedding architecture, and exotic clasts (i.e., Pedernal chert and 10-40% quartzite in petrofacies 3, Tables 3-4) indicate deposition by a through-going Rio Grande — consistent with a quartz vs. feldspar+lithics ratio in the sand fraction that is >1 (based on hand lens inspection). In the following, we discuss how the unique gravel compositions of the LCU petrofacies allow correlation to the general provenance regions introduced above (Figs. 1, 10; Tables 1-4). Gravel of petrofacies 1 contains a high percentage of Mesozoic and Paleozoic sedimentary clasts, with proportions and types similar to the Palomas Formation Mescal-Ash Canyon paleo-alluvial fan and recent alluvium in Mescal and Ash Canyons (Fig. 10; Tables 2-4). The paucity of intermediate volcanic rocks and general abundance of felsic volcanic rocks — together with variable Paleozoic carbonates, green Cretaceous sandstones, and granite — characterize petrofacies 2 of the LCU; these gravel compositions primarily correlate with the north-northeastern provenance region without exotic gravel input from the ancestral Rio Grande.

Petrofacies 3 of the LCU contains relatively high amounts of intermediate volcanic clasts (20-30%) mixed with 10-60% felsic volcanic clasts, common quartzite (10-40%), and low amounts of Paleozoic clasts and green Cretaceous sandstones. The relatively high proportion of intermediate volcanic rocks indicates gravel derivation primarily from the west-northwest provenance region (Table 1; Table 2, S-1 through S-3). A particularly distinctive clast in petrofacies 3, a feldspar-megaphyric porphyry, bolsters correlations to the west-northwest provenance region because cobbles and boulders of that clast type are common in Quaternary terrace deposits alongside Alamosa Creek in the Monticello area. Since quartzite is lacking in the highland source regions, the presence of 10-40% quartzite in petrofacies 3 reflects transport of exotic clasts by the Rio Grande from source areas north of the Engle basin — consistent with the presence of trace Pedernal chert derived from the northwestern Jemez Mountains.

Petrofacies 1 was previously assigned to the Palomas Formation piedmont facies (Lozinsky, 1986), but we interpret it as an axial-fluvial facies that has locally reworked coarse sediment via toe-cutting of the Mescal-Ash Canyon paleofan. Petrofacies 1 exhibits cross-stratification (Figs. 6, 8), consistent with axial-fluvial strata in the northern Palomas basin (e.g., Jochems and Koning, 2015) and in contrast to the very thin to thin, tabular bedded paleo-fan sediment observed on the southern slopes of lower Cuchillo Negro Creek. Moreover, petrofacies 1 appears to contain various proportions of Rio Grande axial-fluvial sand, consistent with intertonguing of this petrofacies with axial-fluvial beds of petrofacies 2. Comparing Mescal-Ash Canyon paleofan sand with sand of petrofacies 1 illustrates this mixing. Petrofacies 1 sand is more rounded than the paleo-fan sand and is light brownish gray to tan (10YR 6/2 and 10YR 7/3; 10YR 6/3-4) rather than the paleofan's bimodal green and reddish (likely a reflection of less green quartz and lithic sandstone grains in petrofacies 1). Detailed petrographic work is planned to better demonstrate the degree of mixing of axial-fluvial vs. Mescal-Ash Canyon sand in petrofacies 1.

Ages of Petrofacies in the Lower Coarse Unit

We argue that the petrofacies 2 was deposited prior to petrofacies 3 in the study area based on stratigraphy, presence vs.

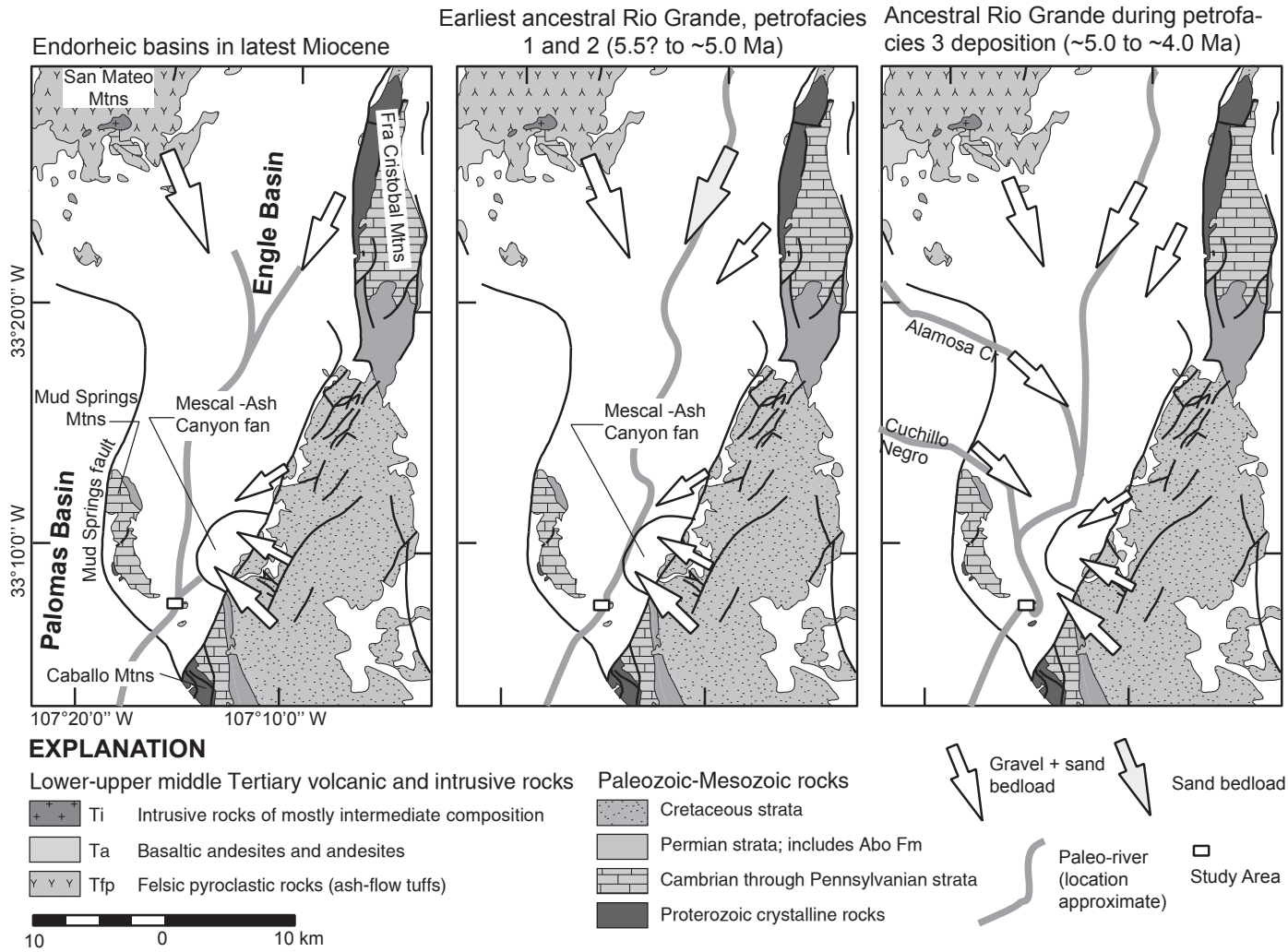


FIGURE 15. Paleogeographic maps depicting fluvial evolution for three different time periods in the latest Miocene and early Pliocene. Arrows are qualitatively scaled according to inferred sediment flux. Note that prior to ~5.0 Ma (approximate minimum age for the petrofacies 3 of the LCU), the Rio Grande did not transport appreciable gravel. Gravel correlated to Alamosa Creek (the marker feldspar-megaphyric porphyry clast) and Cuchillo Negro (high amounts of intermediate volcanic clasts) does not appear until deposition of petrofacies 3.

absence of exotic clasts, and consideration of gravel transport paths (Fig. 15). There are no intertongues of petrofacies 3 within petrofacies 2, and we have not observed petrofacies 2 overlying petrofacies 3 (Fig. 11). In addition, there is no observed mixing of gravel between petrofacies 2 and 3, but there would have to be mixing if the two petrofacies were deposited at the same time. To expound on this latter point, the gravel suite of petrofacies 2 most resembles a mix of rock types exposed in the north-northeastern provenance region. However, except for a single pebble of Pedernal chert found at the very top of the unit at the cryptomelane FZ-2 sample site, petrofacies 2 is distinctly lacking in exotic gravel attributable to northern New Mexico by way of the Rio Grande (i.e., quartzite, Pedernal chert). This indicates that during its deposition the Rio Grande was transporting and mixing gravel from source regions adjacent to the Engle basin southward to the study area, but it was not transporting gravel from northern New Mexico to the study area (Fig. 15). In contrast, the gravel suite in petrofacies 3 consists of material mainly derived from the north-northwest provenance region and also includes gravel attributed to northern New Mexico.

The contrast between petrofacies 2 and 3 gravel compositions cannot be explained solely by local variables, such as the flowpath of the Rio Grande or localized intense storm activity delivering sediment from only select source areas. For example, a major gravel type of petrofacies 2 are felsic volcanic rocks from the southeastern San Mateo Mountains. If northerly-derived exotic gravel was present in the Rio Grande during deposition of petrofacies 2, consideration of transport paths means it would be mixed with gravel of petrofacies 2 (Fig. 15). Because gravel was incorporated into petrofacies 2 from the Fra Cristobal Mountains and Cretaceous highlands to the south, the Rio Grande was not simply shifted east of streams derived from the southeast San Mateo Mountains; rather, streams sourced from the west and east sides of the Engle basin merged upstream of the study area.

Thus, we conclude that the exotic-bearing petrofacies 3 and exotic-lacking petrofacies 2 were deposited at two differ-

ent times in the evolution of the ancestral Rio Grande, with petrofacies 2 deposited first because it underlies petrofacies 3. The fact that petrofacies 3 overlies the base of the LCU in the western study area, which is approximately the same elevation as the LCU base in the eastern study area, is supportive of a paleovalley-related buttress contact (Fig. 11).

At the cryptomelane sample site, the presence vs. absence of manganese cementation in petrofacies 2 and 3 provides a valuable age constraint for their deposition (Figs. 11 and 13). Although cryptomelane sample FZ-2 came from a fault zone in upper Paleozoic rock (Fig. 13C), associated manganese mineralization extends into adjoining petrofacies 2. Thus, the 4.87 Ma cryptomelane age provides a minimum age constraint for preserved petrofacies 2 strata at the site. There is no notable manganese precipitation in the overlying petrofacies 3. Thus, the 4.87 Ma cryptomelane age provides a maximum age constraint for the scoured, disconformable contact and the overlying petrofacies 3 at the site, although this maximum age constraint does not apply to the inferred paleovalley to the west.

The lower to middle part of the inferred paleovalley in the western study area (Fig. 11)was backfilled sometime prior to 4.9 Ma because it contains a tooth identified as *Neohipparion eurystyle*, whose age range extends from ~7.5 to 4.9 Ma. Given the 4.87 Ma age of sample FZ-2 at the cryptomelane site, manganese precipitation at that locale occurred during the aggradation of the upper paleovalley (Fig. 11). After the paleovalley completely backfilled, the river widened or shifted eastward and carved the disconformity seen at the cryptomelane site. Then the Rio Grande deposited ~12 m of petrofacies 3 near the cryptomelane site prior to deposition of the upper axial-fluvial sediment (Figs 4, 11).

Both petrofacies 1 and 2 must pre-date the 4.87 Ma cryptomelane age and pre-date the 4.9 Ma minimum age of *Neohipparion eurystyle*, since the tooth was found in the inferred paleovalley inset into both of these units. We do not have other age constraints for petrofacies 1 and 2. The combined thickness of the two petrofacies is 12-13 m (Fig. 4), which could have been deposited as quickly as 0.06-0.20 Ma using stratal accumulation rates derived from higher in the section (i.e., the 40 m distance between the 3.6-3.3 Ma Repenning locality and the 3.1 Ma Mud Springs pumice; Morgan and Lucas, 2011, 2012). A conservative estimate for the age of earliest Rio Grande sedimentation (represented by lower petrofacies 2 and petrofacies 1) is therefore 5.5(?)-5.0 Ma.

Early Rio Grande Flow and Sedimentation

There is no evidence in the study area of earlier Rio Grande sedimentation in strata older than the LCU unit (i.e., the Rincon Valley Formation). Sand in the Rincon Valley Formation is reddish, relatively angular, and contains less quartz than the light gray to white, generally subrounded, quartz-rich sand in the LCU and higher axial-fluvial strata. The lack of thick cross-stratification and fine gravel sizes in the Rincon Valley Formation suggest relatively low stream power, in contrast to the higher stream power in the LCU indicated by local thick cross-stratification and cobbles. Thus, our estimated 5.5(?)-5.0 Ma age for basal LCU strata would coincide with the arrival of the Rio Grande into the T or C area and the northern Palomas basin.

Preservation of 2-m-thick lateral accretion sets near the Main Street stratigraphic section (Fig. 6) indicates that flow depths during early Rio Grande deposition were ≥2.0-2.5 m, at least periodically. Given the site is interpreted to lie on the basin floor, it is difficult to envision paleoflow derived solely from Mescal or Ash Canyon attaining >2-m flow depths. We thus attribute the extensive cover of the basal LCU contact by petrofacies 1 to toe-cutting of the Mescal-Ash Canyon paleofan by a powerful Rio Grande. Mixing of Mesozoic-Paleozoic clasts in petrofacies 1 with minor (<10%) Proterozoic gneisses (probably from the Fra Cristobal Mountains) and felsic+intermediate volcanic rocks (Tables 3-4) is consistent with fan toe-cutting and mixing of Mescal-Ash Canyon gravel with axial gravel derived from the southeastern San Mateo Mountains and the Fra Cristobals.

Flashy discharge is consistent with meter-scale incision and back-filling events seen in petrofacies 1 immediately east of the Main Street stratigraphic section (Fig. 6). There, subunit 1 is 1.5-2.0 m thick and includes back-filling of a 1-m-deep, narrow scour. Subunit 1 is incised >2 m and back-filled by a second deposit with 2.0- to 2.5-m-thick lateral accretion foresets (Fig. 6). Overlying, at least in part, the associated buttress contact is a colluvial wedge. The colluvial wedge, deep scours, and thick cross-stratification indicate high discharges separated by subaerial exposure.

Stream power in the axial river increased shortly prior to 4.9 Ma, the minimum age of *Neohipparion eurystyle* found in paleovalley deposits of petrofacies 3, and waned sometime between 4.8 and 3.6 Ma. The earlier increase in stream power facilitated paleovalley incision in the western study area and transport of large clasts from northern New Mexico (i.e., quartzites and Pedernal cherts that are up to cobble-size). Waning stream power likely accompanied 30 m of sand-dominated axial-fluvial strata that includes the Repenning fossil site (Fig. 4), which is 3.6-3.3 Ma age (Morgan et al., 2011, 2012).

Although the subject of on-going study, these phenomena are probably best attributed to paleoclimatic-modulated changes in discharges. For example, increased southwest-down displacement rates on the Williamsburg-Mud Springs fault system might drive paleovalley development by lowering base level just downstream of the study area. But, this fault activity alone would not account for the delivery of coarse detritus from northern New Mexico in petrofacies 3. Pronounced paleoclimate change ca. 5 Ma has been inferred from mammalian immigration episodes into North America (Webb and Opdike, 1995) and is consistent with interpretations of an intensified North American monsoon near the Mio-Pliocene transition (Chapin, 2008). Compared to a dry latest Miocene, in which habitats were converting from savanna to arid, largely treeless steppes (Chapin, 2008; MacFadden, 1992; Webb and Opdike, 1995; Latorre et al., 1997), previous workers have suggested a generally high, effective moisture in the early-middle Pliocene (Thompson, 1991) and interpreted a persistent El Niño state during that time (Wara et al., 2005; Ravelo et al., 2006). Future

stratigraphic study and dating efforts in the T or C area and Palomas basin will attempt to relate paleoclimatic and tectonic drivers to ancestral Rio Grande deposition and the river's southward advancement between the Socorro-Albuquerque basins and the El Paso area.

SUMMARY

Based on two age constraints, a 4.87 Ma $^{40}Ar/^{39}Ar$ age from cryptomelane and identification of a fossil tooth (NMMNH 67139) as the three-toed horse *Neohipparion eurystyle* (~7.5-4.9 Ma), we interpret the following fluvial narrative in the study area for 6.0-4.0 Ma (Fig. 15). A south-flowing, low-energy fluvial system connected the Engle and Palomas basins in the latest Miocene and deposited reddish, tabular-bedded sand, pebbly sand, and clayey-silty sand of the Rincon Valley Formation. The ancestral Rio Grande likely advanced into the T or C area between 5.5(?) and 5.0 Ma, toe-cutting the Mescal Canyon alluvial fan and redistributing this gravel as petrofacies 1. Later in the same time frame, the Rio Grande deposited gravel derived from highlands surrounding the Engle basin; this gravel was mixed with extra-basinal, quartz-rich sand (petrofacies 2). Paleoclimate changes are inferred to have increased the competency and stream power of the Rio Grande imediately prior to deposition of petrofacies 3, which began shortly prior to 4.9 Ma, allowing the river to transport cobble-size clasts from both northern New Mexico and mountains surrounding the Engle and northern Palomas basins; this stream power increase also likely induced incision of a paleovalley in the western study area that was bacfilled by petrofacies 3. Fault-controlled manganese mineralization occurred at 4.87 Ma during the latter phases of back-filling of the paleovalley. Stream power appears to have waned between 4.87 and 3.6-3.3 Ma, resulting in deposition of sand-dominated axial-fluvial strata that overlies the LCU.

ACKNOWLEDGMENTS

We thank Glen Johnson for allowing us access to useful exposures on his property. We very much appreciate the thorough manuscript reviews by Colin Cikoski and Brian Hampton, and the field review by Greg Mack and Shari Kelley. Richard C. Hulbert Jr. assisted with the identification of the horse tooth. Funding for field sampling and age dating of the cryptomelane was provided by a grant from Department of Energy-American Association of State Geologists-Arizona Geological Survey for the exploration of blind geothermal systems (NM-0003850).

REFERENCES

Bachman, G.O., and Mehnert, H.H., 1978, New K-Ar dates and the late Pliocene to Holocene geomorphic history of the central Rio Grande region, New Mexico: Geological Society of America Bulletin, v. 89, p. 283-292.

Baldridge, W.S., Damon, P.E., Shafiqullah, M., and Bridwell, R.J., 1980, Evolution of the central Rio Grande rift, New Mexico: New potassium-argon ages: Earth and Planetary Science Letters, v. 51, p. 309-321.

Chamberlin, R.M., 1999, Geologic map of the Socorro quadrangle, Socorro County, New Mexico: New Mexico Bureau of Geology and Mineral Resources, Open-file Geologic Map 034, scale 1:24,000.

Chamberlin, R.M., and Osburn, G.R., 2006, Preliminary geologic map of the Water Canyon quadrangle, Socorro County, New Mexico: New Mexico Bureau of Geology and Mineral Resources, Open-file Geologic Map 118, scale 1:24,000.

Chapin, C.E., 2008, Interplay of oceanographic and paleoclimate events with tectonism during middle to late Miocene sedimentation across the southwestern USA: Geosphere, v. 4, p. 976-991, doi:10.1130/GES00171.1.

Cikoski, C.T., and Koning, D.J., 2013, Geologic map of the Huerfano Hill quadrangle, Sierra County, New Mexico: New Mexico Bureau of Geology and Mineral Resources, Open-file Geologic Map 243, scale 1:24,000.

Cikoski, C.T., Harrison, R.W., Koning, D.J., and Jahns, R.H., 2012 (last modified January-2013), Geologic map of the Iron Mountain quadrangle, Sierra County, New Mexico: New Mexico Bureau of Geology and Mineral Resources, Open-file Geologic Map 229, scale 1:24,000.

Compton, R.R., 1985, Geology in the Field: New York, John Wiley and Sons, 398 p.

Connell, S.D., 2004, Geology of the Albuquerque basin and tectonic development of the Rio Grande rift in north-central New Mexico, *in* Mack, G.H., and Giles, K.A., eds., Geology of New Mexico: A Geologic History: New Mexico Geological Society, Special Publication 11, p. 359-388.

Connell, S.D., Hawley, J.W., and Love, D.W., 2005, Late Cenozoic drainage development in the southeastern Basin and Range of New Mexico, southeasternmost Arizona, and western Texas, *in* Lucas, S.G., Morgan, G.S., and Zeigler, K.E., eds., New Mexico's Ice Ages: New Mexico Museum of Natural History and Science, Bulletin No. 28, p. 125-150.

Denny, C.S., 1940, Tertiary geology of the San Acacia area, New Mexico: Journal of Geology, v. 48, issue 1, p. 73-106.

Farkas, S.E., 1969, Geology of the southern San Mateo Mountains, Socorro and Sierra Counties, New Mexico [Ph.D. dissertation]: Albuquerque, University of New Mexico, 181 p.

Foruria, J., 1984, Geology, alteration, and precious metal reconnaissance of the Nogal Canyon area, San Mateo Mountains, New Mexico [M.S. thesis]: Fort Collins, Colorado State University, 178 p.

Foster, R., 2009, Basin-fill architecture of the Pliocene-Lower Pleistocene Palomas Formation adjacent to the intrabasinal Mud Springs Mountains, southern Rio Grande rift [M.S. thesis]: Las Cruces, New Mexico State University, 81 p.

Furlow, J.W., 1965, Geology of the San Mateo Peak area, Socorro County, New Mexico [M.S. thesis]: Albuquerque, University of New Mexico, 83 p.

Gilmer, A.L., Mauldin, R.A., and Keller, G.R., 1986, A gravity study of the Jornada del Muerto and Palomas basins: New Mexico Geological Society, Guidebook 37, p. 131-134.

Harrison, R.W., 1992, Cenozoic stratigraphy, structure, and epithermal mineralization of north-central Black Range, New Mexico, in the regional geologic framework of south-central New Mexico [Ph.D. dissertation]: Socorro, New Mexico Institute of Mining and Technology, 444 p.

Harrison, R.W., and Cikoski, C.T., 2012, Geologic map of the Winston quadrangle, Sierra County, New Mexico: New Mexico Bureau of Geology and Mineral Resources, Open-file Geologic Map 230, scale 1:24,000.

Harrison, R.W., Lozinsky, R.P., Eggleston, T.L., and McIntosh, W.C., 1986, Geologic map of the Truth or Consequences 30 x 60 minute quadrangle (1:100,000 scale): New Mexico Bureau of Mines and Mineral Resources, Open-file Report 390, 20 p.

Hermann, M.L., 1986, Geology of the southwestern San Mateo Mountains, Socorro County, New Mexico [M.S. thesis]: Socorro, New Mexico Institute of Mining and Technology, 192 p.

Heyl, A.V., Maxwell, C.H., and Davis, L.L., 1983, Geology and mineral deposits of the Priest Tank quadrangle, Sierra County, New Mexico: U.S. Geological Survey, Miscellaneous Field Studies Map MF-1665, scale 1:24,000.

Houser, B. B., 1987, Geologic map of the Alma quadrangle, Catron County, New Mexico: U. S. Geological Survey, Map GQ-1610.

Hulbert, R.C., Jr., 1987, Late Neogene *Neohipparion* (Mammalia, Equidae) from the Gulf Coastal Plain of Florida and Texas: Journal of Paleontology, v. 61, p. 809-830.

Jahns, R.H., 1955, Geology of the Sierra Cuchillo, New Mexico: New Mexico Geological Society, Guidebook 6, p. 158–174.

Jahns, R.H., McMillan, K., and O'Brient, J.D., 2006, Geologic map of the Chise quadrangle, Sierra County, New Mexico: New Mexico Bureau of Geology and Mineral Resources, Open-file Geologic Map 115, scale

1:24,000.

Jochems, A.P., and Koning, D., 2015, Geologic map of the Williamsburg 7.5-minute quadrangle, Sierra County, New Mexico: New Mexico Bureau of Geology, Open-file Geologic Map 250, scale 1:24,000.

Kelley, S.A., Kempter, K.A., McIntosh, W.C., Maldonado, F., Smith, G.A., Connell, S.D., Koning, D.J., and Whiteis, J., 2013, Syndepositional deformation and provenance of Oligocene to lower Miocene sedimentary rocks along the western margin of the Rio Grande rift, Jemez Mountains, New Mexico, *in* Hudson, M., and Grauch, V.J.S., eds., New Perspectives on the Rio Grande Rift: From Tectonics to Groundwater: Boulder, Geological Society of America, Special Paper 494, p. 101-123, doi:10.1130/2013.2494(05).

Kelley, V.C., and Silver, C., 1952, Geology of the Caballo Mountains: University of New Mexico, Publications in Geology, no. 5, 286 p.

Koning, D.J., Jochems, A.P., and Cikoski, C., 2015, Geologic map of the Skute Stone Arroyo 7.5-Minute quadrangle, Sierra County, New Mexico: New Mexico Bureau of Geology and Mineral Resources, Open-file Geologic Map 252, scale 1:24,000.

Koning, D.J., Jochems, A., Kelley, S.A., McLemore, V.T., and Cikoski, C.T., 2014, Geologic map of the Monticello 7.5-Minute quadrangle, Sierra and Socorro Counties, New Mexico: New Mexico Bureau of Geology and Mineral Resources, Open-file Geologic Map 245, scale 1:24,000.

Kottlowski, F.E., 1953, Tertiary-Quaternary sediments of the Rio Grande Valley in southern New Mexico: New Mexico Geological Society, Guidebook 4, p. 144-148.

Kottlowski, F.E., 1958, Geologic history of the Rio Grande near El Paso: West Texas Geological Society Guidebook, p. 46-54.

Kottlowski, , F.E., Cooley, M.E., and Ruhe, R.V., 1965, Quaternary geology of the Southwest, *in* Wright, H.E., Jr., and Frey, D.G., eds., The Quaternary Geology of the United States: Princeton, Princeton University Press, p. 287-298.

Kuiper, K.F., Deino, A., Hilgen, F.J., Krijgsman, W., Renne, P.R., and Wijbrans, J.R., 2008, Synchronizing rock clocks in Earth history: Science, v. 320, p. 500-504.

Latorre, C., Quade, J., and McIntosh, W.C., 1997, The expansion of C4 grasses and global change in the late Miocene: Stable isotope evidence from the Americas: Earth and Planetary Science Letters, v. 146, p. 83-96.

Lozinsky, R.P., 1986, Geology and late Cenozoic history of the Elephant Butte area, Sierra County, New Mexico: New Mexico Bureau of Mines and Mineral Resources, Circular 187, 39 p.

Lozinsky, R.P., 1987, Cross section across the Jornada del Muerto, Engle, and northern Palomas Basins, south-central New Mexico: New Mexico Geology, v. 9, p. 55-57 and p. 63.

Lozinsky, R.P., and Hawley, J.W., 1986a, The Palomas Formation of south-central New Mexico—A formal definition: New Mexico Geology, v. 8, p. 73–82.

Lozinsky, R.P., and Hawley, J.W., 1986b, Upper Cenozoic Palomas Formation of south-central New Mexico: New Mexico Geological Society, Guidebook 37, p. 239–247.

Lucas, S.G., and Oakes, W., 1986, Pliocene (Blancan) vertebrates from the Palomas Formation, south-central New Mexico: New Mexico Geological Society, Guidebook 37, p. 249-263.

Lueth, V.W., 2012, The Ellis manganese deposits at Truth or Consequences, New Mexico: a link between hot springs and ore deposits: New Mexico Geological Society, Guidebook 37, p. 126-128.

Lueth, V.W., Peters, L., and Chamberlin, R., 2004, $^{40}Ar/^{39}Ar$ age dating of hydrothermal manganese mineralization in the Luis Lopez district, New Mexico: New Mexico Bureau of Mines and Mineral Resources, Bulletin 161, p. 239-249.

MacFadden, B.J., 1984, Systematics and phylogeny of *Hipparion, Neohipparion, Nannippus,* and *Cormohipparion* (Mammalia, Equidae) from the Miocene and Pliocene of the New World: Bulletin of the American Museum of Natural History, v. 171, p. 1-195.

MacFadden, B.J., 1992, Fossil Horses: Systematics, Paleobiology, and Evolution of the Family Equidae: New York, Camridge University Press, 369 p.

Machette, M.N., Personius, S.F., Kelson, K.I., Dart, R.L., and Haller, K.M., 1998, Map and data for Quaternary faults and folds in New Mexico: U.S. Geological Survey, Open-file Report 98-521 (electronic version), 358 p. and 1 plate.

Mack, G.H., Dunbar, N., and Foster, R., 2009, New sites of 3.1-Ma Pumice beds in axial-fluvial strata of the Camp Rice and Palomas Formations, southern Rio Grande rift: New Mexico Geology, v. 31, p. 31–37.

Mack, G.H., Foster, R., and Tabor, N.J., 2012, Basin architecture of Pliocene-lower Pleistocene alluvial-fan and axial-fluvial strata adjacent to the Mud Springs and Caballo Mountains, Palomas half graben, southern Rio Grande rift: New Mexico Geological Society, Guidebook 63, p. 431-445.

Mack, G.H., Love, D.W., and Seager, W.R., 1997, Spillover models for axial rivers in regions of continental extension: The Rio Mimbres and Rio Grande in the southern Rio Grande rift, USA: Sedimentology, v. 44, p. 637-652.

Mack, G.H., McIntosh, W.C., Leeder, M.R., and Monger, H.C., 1996, Plio-Pleistocene pumice floods in the ancestral Rio Grande, southern Rio Grande rift, USA: Sedimentary Geology, v. 103, p. 1-8.

Mack, G.H., Salyards, S.L., and James, W.C., 1993, Magnetostratigraphy of the Plio-Pleistocene Camp Rice and Palomas Formations in the Rio Grande rift of southern New Mexico: American Journal of Science, v. 293, p. 49–77.

Mack, G.H., Salyards, S.L., McIntosh, W.C., Leeder, M.R., 1998, Reversal magnetostratigraphy and radioisotopic geochronology of the Plio-Pleistocene Camp Rice and Palomas formations, southern Rio Grande rift: New Mexico Geological Society, Guidebook 49, p. 229–236.

Mack, G.H., Seager, W.R., and Kieling, J., 1994, Late Oligocene and Miocene faulting and sedimentation, and evolution of the southern Rio Grande rift, New Mexico, USA: Sedimentary Geology, v. 92, p. 79-96.

Mack, G.H., Seager, W.R., Leeder, M.R., Perez-Arlucea, M., and Salyards, S.L., 2006, Pliocene and Quaternary history of the Rio Grande, the axial river of the southern Rio Grande rift, New Mexico, USA: Earth-Science Reviews, v. 79, p. 141–162.

Maldonado, F., 1980, Geologic map of the northern part of the Sierra Cuchillo, Socorro and Sierra Counties, New Mexico: U.S. Geological Survey, Open-file Report 80-230, scale 1:24,000.

Manley, K., 1979, Stratigraphy and structure of the Española basin, Rio Grande rift, New Mexico, *in* Riecker, R.E., ed., Rio Grande Rift,: Tectonics and Magmatism: Washington, D.C., American Geophysical Union, p. 71-86.

Mason, J.T., 1976, The geology of the Caballo Peak quadrangle, Sierra County, New Mexico [M.S. thesis]: Albuquerque, University of New Mexico, 131 p.

Maxwell, C.H., and Oakman, M.R., 1990, Geologic map of the Cuchillo quadrangle, Sierra County, New Mexico: U. S. Geological Survey, Geologic Quadrangle Map GQ-1686, scale 1:24,000.

McCleary, J.T., 1960, Geology of the northern part of the Fra Cristobal Range, Sierra and Socorro Counties, New Mexico [M.S. thesis]: Albuquerque, University of New Mexico, 59 p. and 1 sheet.

McLemore, V.T., 2010, Geology, mineral resources, and geoarchaeology of the Montoya Butte quadrangle, including the Ojo Caliente No. 2 Mining District, Socorro County, New Mexico: New Mexico Bureau of Geology and Mineral Resources, Open-file Report 535, 106 p.

Morgan, G.S., 2015, Late Cenozoic vertebrate faunas from the Gila Region of southwestern New Mexico: Proceedings of the Fourth Natural History of the Gila Symposium, The New Mexico Botanist, Special Issue Number 4, p. 77-105.

Morgan, G.S., and Lucas, S.G., 2003, Mammalian biochronology of Blancan and Irvingtonian (Pliocene and early Pleistocene) faunas from New Mexico: Bulletin of the American Museum of Natural History, no. 278, p. 269-320.

Morgan, G.S., and Lucas, S.G., 2011, *Stegomastodon* (Mammalia: Proboscidea: Gomphotheriidae) from the Blancan and Irvingtonian (Pliocene and early Pleistocene) of New Mexico: New Mexico Museum of Natural History and Science Bulletin 53, p. 570-582.

Morgan, G.S., and Lucas, S.G., 2012, Cenozoic vertebrates from Sierra County, southwestern New Mexico: New Mexico Geological Society, Guidebook 63, p. 525-540.

Morgan, G.S., Sealey, P., and Lucas, S.G., 2011, Pliocene and early Pleistocene (Blancan) vertebrates from the Palomas Formation in the vicinity of Elephant Butte Lake and Caballo Lake, Sierra County, southwestern New Mexico: New Mexico Museum of Natural History and Science, Bulletin 53, p. 664-736.

Morgan, G. S., Sealey, P. L., Lucas, S. G., and Heckert, A, B., 1997, Pliocene (latest Hemphillian and Blancan) vertebrate fossils from the Mangas basin, southwestern New Mexico: New Mexico Museum of Natural Histo-

ry and Science, Bulletin 11, p. 97-128.
Nelson, W.J., Lucas, S.G., Krainer, K., McLemore, V.T., and Elrick, S., 2012, Geology of the Fra Cristobal Mountains, New Mexico: New Mexico Geological Society, Guidebook 63, p. 195-210.
NMBGMR [New Mexico Bureau of Geology and Mineral Resources], 2003, Geologic Map of New Mexico: New Mexico Bureau of Geology and Mineral Resources, scale 1:500,000.
Ogg, J.G., 2012, Geomagnetic polarity time scale, *in* Gradstein, F.M., Ogg, J.G., Schmitz, M.D., and Ogg, G.M., eds., The Geologic Time Scale 2012: Berlin, Elsevier, p. 31-42.
Osburn, G.R., compiler, 1984, Socorro county geologic map: New Mexico Bureau of Mines and Mineral Resources Open-File Report 238, 14 p., 1 sheet.
Ratté, J.C., and Finnell, T.L., 1978, Third day road log from Silver City to Reserve via Glenwood and the Mogollon Mining District: New Mexico Geological Society, Special Publication 7, p. 49-63.
Ravelo, A.C., Dekens, P.S., and McCarthy, M., 2006, Evidence for El Niño-like conditions during the Pliocene: GSA Today, v. 16, no. 3, p. 4-11, doi: 10.1130/1052-5173(2006)016<4:EFENLC>2.0.CO;2.
Repenning, C.A., and May, S.R., 1986, New evidence for the age of the lower part of the Palomas Formation, Truth or Consequences, New Mexico: New Mexico Geological Society, Guidebook 37, p. 257-260.
Ruhe, 1962, Age of the Rio Grande Valley in southern New Mexico: Journal of Geology, v. 70, issue 2, p. 151-167.
Seager, W.R., Hawley, J.W., and Clemons, R.E., 1971, Geology of San Diego Mountain area, Doña Ana County, New Mexico: New Mexico Bureau of Mines and Mineral Resources, Bulletin 97, 38 p. and 2 plates.
Seager, W.R., and Mack, G.H., 2003, Geology of the Caballo Mountains, New Mexico: New Mexico Bureau of Geology and Mineral Resources, Memoir 49, 136 p.
Seager, W.R., Mack, G.H., and Lawton, T.F., 1997, Structural kinematics and depositional history of a Laramide uplift-basin pair in southern New Mexico: Implications for development of intraforeland basins: Geological Society of America Bulletin, v. 109, p. 1389-1401.
Seager, W.R., Shafiqullah, M., Hawley, J.W., and Marvin, R.F., 1984, New K-Ar dates from basalts and the evolution of the southern Rio Grande rift: Geological Society of America Bulletin, v. 95, p. 87–99.
Smith, G.A., 2004, Middle to late Cenozoic development of the Rio Grande rift and adjacent regions in northern New Mexico, *in* Mack, G.H., and Giles, K.A., eds., The Geology of New Mexico, A Geologic History: New Mexico Geological Society, Special Publication 11, p. 331-358.
Smith, G.A., McIntosh, W., and Kuhle, A.J., 2001, Sedimentologic and geomorphic evidence for seesaw subsidence of the Santo Domingo accommodation-zone basin, Rio Grande rift, New Mexico: Geological Society of America Bulletin, v. 113, p. 561-574.
Tedford, R.H., 1981, Mammalian biochronology of the Late Cenozoic basins of New Mexico: Geological Society of America Bulletin, v. 92, p. 1008-1022.
Thompson, R.S., 1991, Pliocene environments and climates in the western United States: Quaternary Science Reviews, v. 10, p. 115-132.
Thompson, S., III, 1955, Geology of the southern part of the Fra Cristobal Range, Sierra County, New Mexico [M.S. thesis]: Albuquerque, University of New Mexico, 67 p.
Timmer, R.S., 1976, Geology and sedimentary copper deposits in the western part of the Jarosa and Seven Springs quadrangles, Rio Arriba and Sandoval Counties, New Mexico [M.S. thesis]: Albuquerque, University of New Mexico, 151 p.
Udden, J.A., 1914, The mechanical composition of clastic sediments: Geological Society of America Bulletin, v. 25, p. 655-744.
Vasconcelos, 1999, K-Ar and $^{40}Ar/^{39}Ar$ geochronology of weathering processes: Annual Reviews of Earth and Planetary Sciences, v. 27, p. 183-229.
Wara, M.W., Ravelo, A.C., and Delaney, M.L., 2005, Permanent El Nino-like conditions during the Pliocene warm period: Science, v. 309, p. 758-761, doi:10.1126/science.1112596.
Webb, S.D., and Opdyke, N.D., 1995, Global climatic influence on Cenozoic land mammal fauna, *in* Effects of Past Global Change on Life: Washington, D.C., National Academy Press, p. 184-208.
Wentworth, C.K., 1922, A scale of grade and class terms for clastic sediments: Journal of Geology, v. 30, p. 377-392.

Supplemental data can be found at http://nmgs.nmt.edu/repository/index.cfml?rid=2016005